The effect of ICRF and LHCD waveguide and launcher location on tritium breeding ratio and radiation damage in fusion reactors

By

Jennifer Marie Sierchio

B.S., University of Arizona (2011)

S.M., Massachusetts Institute of Technology (2014)

Submitted to the Department of Nuclear Science and Engineering
in partial fulfillment for the requirements for the degree of
Master of Science in Nuclear Science and Engineering
at the

MASSACHUSETTS INSTITUTE OF TECHNOLOGY

February 2016

Signature of Author . . . . . Signature redacted

Department of Nuclear Science and Engineering

January 15, 2016

Certified by . . . . . Signature redacted

Dennis G. Whyte

Department Head and Professor of Nuclear Science and Engineering

Thesis supervisor

Certified by . . . . . Signature redacted . . . . . .

Michael Short

Assistant Professor of Nuclear Science and Engineering

Thesis Reader

Accepted by . . . . . Signature redacted . . . . . .

Ju Li

Battelle Energy Alliance Professor of Nuclear Science and Engineering

Chair, Department Committee on Graduate Students

The effect of ICRF and LHCD waveguide and launcher location on tritium breeding ratio and radiation damage in fusion reactors

by

Jennifer Marie Sierchio

Submitted to the Department of Nuclear Science and Engineering
on January 15, 2016, in partial fulfillment of the
requirements for the degree of
Master of Science in Nuclear Science and Engineering

Abstract

In most tokamak fusion reactor designs, ICRF (Ion Cyclotron Range of Frequencies) and LH (Lower Hybrid) radio frequency (RF) waves used to heat the plasma and drive current are launched from the low-field, outboard side where there is more access space. It has recently been proposed to launch these waves from the high-field side [1-3], which increases current-drive efficiency, allows for better wave penetration, and has favorable scrape-off-layer and plasma-material interaction characteristics [4]. However the poloidal location and size of RF launchers will also affect important aspects of the neutronics of the tokamak fusion design, i.e. how the 14.1 MeV neutrons born out of the deuterium-tritium (D-T) fusion reaction interact with the surrounding blanket and structures. The goal of this thesis is to assess the dependence of RF launcher poloidal location on the important neutronics parameters of tritium fuel breeding, launcher damage and activation.

To determine the effects of waveguide and antenna location on Tritium Breeding Ratio (TBR), damage, and activation, the MCNP Transport Code was used, as well as the EASY 2010 activation package to analyze the activation of the vacuum vessel components. A simple geometry was designed for MCNP, based on the original ARC model [1]. Seven locations for the waveguides and antenna were chosen: the inner and outer midplane, the inner and outer upper corners, two spaces between the midplane (inboard and outboard), and a central location directly above the vacuum vessel. TBR, DPA, and helium concentration were calculated at all seven points to find the optimal location for the waveguides and antenna. Four blanket materials were chosen: two liquid blankets (FliBe and Pb-17Li) and two solid blankets (Li_4SiO_4 and Li_2TiO_3). This was to test whether or not blanket material affects the optimal location of the launchers.

We find that from the neutronics point of view the overall optimal location is the inboard upper corner, which minimizes DPA and helium concentration in the antenna and waveguide, and maximizes TBR. DPA in the waveguide was minimized when placed in the outboard upper corner, although the difference in DPA between the two locations was small. While TBR was maximized at the top of the vacuum vessel, the differences in TBR between all locations was less than 1%. These results reinforce the choice of inside, upper corner launch as the optimal location for current drive, launcher protection and neutronics.

Activation was also assessed for the vacuum vessel, both without and with the waveguides and antenna, assuming irradiation times of one week, one month, and one year. Overall, activation was significant in the vacuum vessel, as expected, due to the use of Inconel 718. The IAEA recycling limit could be achieved, regardless of irradiation time. The dominant isotopes present after irradiation differed when the irradiation time was one week versus one month or one year. Activation was also assessed in the waveguides and antenna for the cases of the launchers being placed at the outboard midplane versus the inboard corner. The activation in the antenna was shown to be reduced by a factor of two and in the waveguides by a factor of four, when the launchers were placed in the inboard corner.

Thesis supervisor: Dennis G. Whyte

Title: Professor and Head of the Department of Nuclear Science and Engineering

Thesis reader: Michael Short

Title: Assistant Professor of Nuclear Science and Engineering

Acknowledgments

I would like to thank Professor Dennis Whyte for supervising this thesis, and Professor Michael Short for serving as thesis reader. Their comments and suggestions throughout the research for this work as well as for the thesis itself have proved invaluable.

My parents and brother deserve a tremendous amount of gratitude for their constant support during graduate school and for reminding me of what actually matters in this life.

Ian Faust, Jude Safo, Caleb Waugh, and Dan Kwak – true friends are there even when things get tough. Thank you for being true friends.

Last, but certainly not least, I would like to thank Adam Brooks for his unwavering love and support during my time at MIT. You are simply the best, and I cannot wait to begin our adventure together.

This research was funded, in part, by the National Science Foundation Graduate Research Fellowship Program.

Contents

List of Figures

List of Tables

Chapter 1

Introduction

In most tokamak fusion reactor designs, ICRF (Ion Cyclotron Range of Frequencies) and LH (Lower Hybrid) radio frequency (RF) waves used to heat the plasma and drive current are launched from the low-field, outboard side where there is more access space. It has recently been proposed to launch these waves from the high-field side [1-3], which increases current-drive efficiency, allows for better wave penetration, and has favorable scrape-off-layer and plasma-material interaction characteristics [4]. However the poloidal location and size of RF launchers will also affect important aspects of the neutronics of the tokamak fusion design, i.e. how the 14.1 MeV neutrons born out of the deuterium-tritium (D-T) fusion reaction interact with the surrounding blanket and structures. The goal of this thesis is to assess the dependence of RF launcher poloidal location on the important neutronics parameters of tritium fuel breeding, launcher damage and activation. This introductory chapter is organized as follows. In Section 1.1, the overall motivation for studying fusion is discussed and the optimal plasma geometry and operating conditions is described. In Section 1.2, a generic fusion reactor design is presented, emphasizing energy extraction mechanisms and damage to the reactor. In Section 1.3, the details of the heating and current drive mechanisms necessary for fusion reactor operation are described. Finally in Section 1.4, the discussion is focused onto the problem of how waveguide location affects the energy extraction and materials damage and the rest of the thesis is motivated.

1.1 Fusion energy and tokamaks

Global climate change, specifically warming due to carbon emissions, and an ever-growing world population looking to industrialize (and consume vast amounts of energy) are two of the most significant issues defining the 21st century. To combat these problems, people are searching for cleaner, more abundant, and more efficient sources of energy.

A possible solution for the world's growing energy and climate crises is thermonuclear fusion. Scientists have studied fusion as a possible energy source for over sixty years; it is the same process that allows the Sun and all stars to emit light. Fusion occurs when two light atoms "fuse" together to form a heavier atom that is lighter than the sum of the original two. Because of this mass defect between the reactants and the product, kinetic energy is released.

The most relevant reaction for the purposes of practical energy generation involves isotopes of hydrogen, namely deuterium (D) and tritium (T), fusing to form a helium nucleus and a neutron. This D-T reaction has the highest probability of occurring of any hydrogen fusion reaction and is given below [5]:

$$D + T \rightarrow \alpha + n + 17.6\,MeV, \tag{1.1}$$

Kinematics dictates that the alpha particle (helium nucleus) has 1/5 of the total released energy, or 3.5 MeV, and the neutron has 4/5 of the released energy, or 14.1 MeV. Deuterium is very abundant in Earth's oceans; therefore a readily accessible and inexhaustible supply exists. However, tritium is not naturally abundant in any significant quantity due to its 12.3-year half-life, and thus must be bred by a fusion reactor in a closed fuel cycle within a blanket surrounding the vacuum vessel containing the plasma. Neutrons as products from the original fusion reactions will react with lithium to produce tritons and alphas through two reactions [5]:

$$n(\text{fast}) + {}^{7}_{3}Li \rightarrow T + \alpha + n(slow) - 2.5MeV, \tag{1.2}$$

$$n(\text{thermal}) + {}^{6}_{3}Li \rightarrow \alpha + T + 4.8\ \text{MeV}. \tag{1.3}$$

The breeding process will be described in more detail in Section 1.3 and in Chapters 2 and 4.

The fusion of atoms requires extremely high temperatures to provide net energy, on the order of 100 million Kelvin for hydrogen. At these temperatures, the atoms are completely ionized, with the electrons normally in the atoms no longer bound by the Coulombic attraction of their respective nuclei. These free nuclei (ions) and electrons form what is called a plasma [5, 6].

In our Sun, this plasma is confined by gravity; on Earth, we do not have the mass to confine a plasma gravitationally so we must find other means of confinement.

On way to confine plasmas is by using magnetic fields, since charged particles gyrate around the field lines [6]. As one might expect, not all configurations of magnetic field lines will fully confine the plasma. The most successful configuration, a shaped torus called a tokamak, has magnetic fields both the toroidal and the poloidal directions, as shown in Figure 1.1.

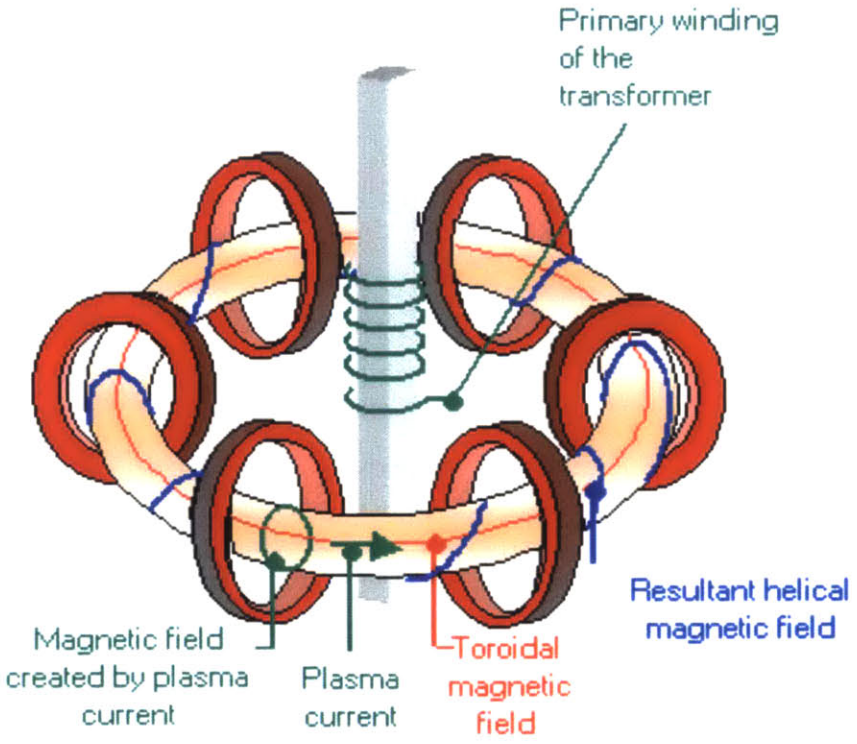

Figure 1.1: Schematic of the coils generating the toroidal and poloidal magnetic fields. Figure from CEA [7].

The toroidal direction is defined to be around the torus the long way; this direction circles around the device when viewing the device from above. The tokamak plasma has the feature that it is symmetric in the toroidal direction, significantly simplifying its analysis and construction. The poloidal direction is the direction around the torus the short way. If we were to look at a cross section of the torus, not as viewed from above but as sideways, the poloidal direction would follow the lines forming the cross-section on one side of the torus, as shown in Figure 1.2. Notice that the poloidal cross-section need not be circular, and often have a soft D-shape. The

toroidal magnetic field is generated by large field coils outside the vacuum vessel stabilizing the plasma as shown in Figure 1.1. The poloidal magnetic field is primarily generated by the plasma current (with additional coils for shaping and position stability).

Looking at the cross section in Figure 1.2, the center of the plasma is located as a radius we call the major radius, R, if we are measuring from the central axis. We can also define a minor radius, r, to be half the maximum horizontal length of the poloidal cross section. So overall, this geometry defines two directions, R and r, and two angles ϕ in the toroidal direction and θ in the poloidal direction. The radius of the tokamak at the outboard (outer or larger R) side is greater, by definition, than it is on the inboard (inner or smaller R) side. Drawing a horizontal line from the central axis of the torus through the center of the plasma extending to the outboard side, and then rotating it around the central axis defines what is known as the midplane. [8]

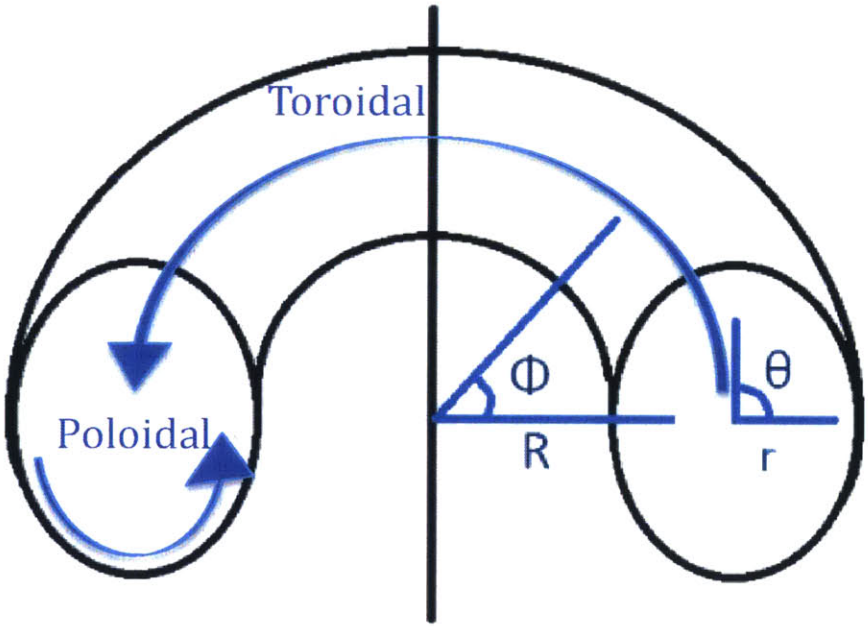

Figure 1.2: Tokamak cross-section with minor (r) and major (R) radial directions, and poloidal (θ) and toroidal (ϕ) angles labeled. The central axis (or major axis of symmetry) is the vertical line down the middle [8]. The major radius (R) goes from the central axis to the center of the plasma.

1.2 Fusion energy extraction: general reactor design

We recall that fuel for the D-T reactions is deuterium obtained from ocean water, and tritium that must be bred through neutron reactions with lithium in a blanket surrounding the plasma vacuum vessel. All neutrons, which are unconfined by the magnetic field, leave the plasma at 14.1 MeV; ostensibly these fast neutrons will react with lithium-7 in Equation 2. Upon first consideration, this seems to be reasonable since lithium-7 makes up 92.5% of natural lithium [9]. However, this endothermic reaction uses almost 18% of the initial kinetic energy of the neutron, which needs to be extracted for the purposes of generating electricity, and the neutrons are disallowed from this reaction after only a few collisions. The exothermic lithium-6 reaction, however, releases an extra 4.8 MeV of energy, but requires thermalized neutrons [5]. At the very least, the blanket needs to include some mix of lithium-6 and lithium-7.

The blanket also needs to moderate neutrons, for multiple reasons. First is that slow neutrons react with lithium-6 to release net energy, thus increasing the energy released from 17.6 MeV to around ~22 MeV. Second is that, without moderation and capture, neutrons will cause damage to the surrounding materials in the form of swelling from combined radiation damage clustering and helium retention. This damage can severely affect balance of plant and plant lifetime. For example, in the case of waveguides and antennas, damage will reduce the efficiency of RF energy transfer (e.g. due to increases in electrical conductivity), requiring more external power to heat the plasma and lowering the fusion plant's gain. Even more detrimental, significant neutron damage can change the internal structure of the superconducting materials used in the toroidal field coils (to provide a continuous magnetic field), causing them to no longer superconduct after some critical neutron fluence is reached. This effectively shortens plant lifetime. Thus our blanket also needs to moderate neutrons and shield the superconductor toroidal field magnets.

Finally, the neutrons deposit their energy in the blanket in the form of heat. This heat must be extracted and converted to electricity with a heat exchanger and generator. The extraction process requires removal of the blanket, the specifics of which depend on whether the blanket is a liquid or solid. If liquid, the liquid will flow out of the reactor at some rate, the same

rate at which fresh blanket flows in. If solid, the reactor must be opened and the solid components must be removed and replaced.

Moving outward in the minor radius direction from the plasma, a fusion reactor contains a plasma surrounded by a first wall typically made of an erosion-resistant materials such as tungsten. Next comes the blanket composed of lithium and other moderating materials. If solid, the blanket requires no other structural materials and resides inside a vacuum vessel. If the blanket is liquid, then there must be a vacuum vessel in between the first wall and the blanket, usually a steel alloy. The liquid blanket must be held in some tank with pipes to allow flows in and out. Beyond the tank must be insulation and the cryostat containing the magnetic field coils, along with . An example of this arrangement is shown in Figure 1.3

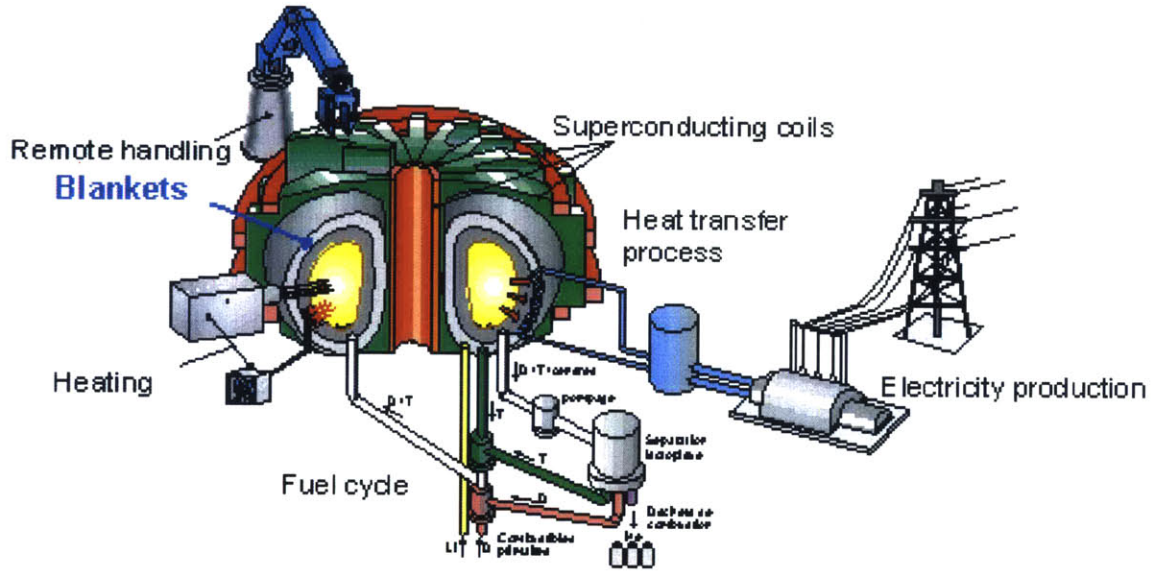

Figure 1.3. General diagram of a full fusion power plant, with a blanket, superconducting magnets and electricity generation. From CEA [10].

1.3 Heating and current drive in tokamaks

As mentioned previously, the probability of the D-T reaction occurring maximizes at high temperatures. This actually creates two problems that must be solved: 1) heating the plasma, and 2) containing it. Regarding the former, ideally the charged alpha particles to be confined so they may transfer their energy to the rest of the plasma. If the plasma is ignited, the alpha particles

provide all the heating necessary to maintain plasma temperature. In reality there is a finite amount of external heating provided to the plasma to both maintain temperature (through heating), and control, through manipulation of the plasma's equilibrium. Regarding the latter, along with a toroidal magnetic field, a poloidal magnetic field generated by current in the plasma itself provides the rotational transform necessary for confinement. In a tokamak operating continuously, one must externally drive a significant fraction of the plasma current. Thus in a tokamak configuration, the heating applied to drive the current is a fundamental design choice which is central to determining the power gain of the fusion reactor.

Fortunately, multiple ways to heat the plasma have been proposed and whose viability continues to be shown through current experiments. The most common heating mechanisms include neutral beams and waves launched into the plasma that damp onto particles at certain resonant frequencies (namely, the ion cyclotron frequency and the lower hybrid frequency which are discussed below). Neutral beams will not be discussed further since large ports at the outboard midplane have to be constructed to launch the beams. This leaves many free streaming neutrons, which will be shown later to cause damage the outer materials and magnets.

By excluding neutron beams, this leaves wave launching as a viable option. Briefly, we will introduce the main types of waves used and general waveguide and antenna design, which will be relevant later in the thesis. We will focus on two waves in particular: the lower hybrid range of frequencies (LH) and the ion cyclotron range of frequencies (ICRF). The reader is referred to [10] for a derivation of these frequencies.

Wave damping in the LH range of frequencies has been found to be effective for current drive. The LH frequency, ω_{LH}, is given by solving [11]:

$$1 + \frac{\omega_{pe}^2}{\omega_{ce}^2} - \frac{\omega_{pi}^2}{\omega_{LH}^2} = 0, \tag{1.4}$$

where ω_{pe} is the electron plasma frequency, ω_{pi} is the ion plasma frequency, and ω_{ce} is the electron cyclotron frequency. These are given by [5]:

$$\omega_{pe}^e = \frac{n_e e^2}{m_e \epsilon_0}, \omega_{pi}^e = \frac{n_i (Ze)^2}{m_i \epsilon_0}, \tag{1.5}$$

$$\omega_{ce} = \frac{eB}{m_e}, \omega_{ci} = \frac{ZeB}{m_i}. \tag{1.6}$$

where n is the density of the electrons or ions, Z is the charge of the ions, m is the mass of the electrons or the ions in kg, B is the magnetic field strength in T, and ϵ_0 is the permittivity of free space, 8.85×10^{-12} F/m. The current drive efficiency is usually written as a figure of merit [11]:

$$\eta = \frac{(\frac{n}{10^{20}\mathrm{m}^{-3}})(\frac{I}{MA})R}{\frac{P}{MW}}, \tag{1.7}$$

where I is the plasma current driven by the heating mechanism, R is the major radius of the tokamak, and P is the absorbed power.

The ICRF frequencies used for plasma heating are given above in Equation 1.10, and are typically on the order of 50-100 MHz due to the fact that toroidal magnetic fields of greater than 4 T are generally considered necessary to produce a fusion reactor. The typical value of the LH frequency in magnetic fusion plasmas is 1-10 GHz and efficiencies of 20-50% can be obtained.

Both LH and ICRF launchers need to be close to the plasma due to the presence of cutoff regions, i.e. locations is plasma parameter space whereby their dispersion relationships are not allowed to propagate in the plasma. Note that vacuum propagation of these ICRF and LH waves is not permitted since the RF frequency is substantially below the electron plasma frequency. The antennas are thus placed inside the vacuum vessel containing the plasma such that they are close in minor radius position to the periphery of the fusion plasma. Current designs place both the antennas and the waveguides that carry the RF power at the outboard midplane for easier geometric access. As will be shown later, this placement is not the ideal location for a variety of reasons.

1.4 Motivation for this thesis

In most fusion reactor designs, ICRF and LH radio frequency waves used to heat the plasma and drive current are launched from the low-field, outboard side where there is more access space. As mentioned above, it has been recently proposed to launch these waves from the high-field side [1-3], which increases current drive efficiency, allows for better wave penetration, and has favorable scrape-off-layer and plasma-material interaction characteristics [4]. The recently-published ARC (Affordable, Robust, Compact) Fusion Nuclear Science Facility (FNSF) design

implements high-field side launch through a vacuum vessel within a liquid immersion blanket [1]. ARC will be further discussed in the next chapter.

As discussed above, one major consequence of high-energy neutrons is damage to materials. This is particularly problematic for the heating and current drive waveguides and antennas that must be very close to the plasma for proper wave penetration; they will be exposed to a high-energy neutron environment without much shielding. This may be mitigated somewhat for the waveguides by placing them further into the blanket. This has the disadvantage of taking up space in the blanket which could be used to breed tritium and moderate neutrons to protect the toroidal field magnets.

This thesis will address how high-field-side launchers and antennas compare to traditional low-field-side launchers and antennas in terms of tritium breeding efficiency and radiation-induced damage. To accomplish this, we will need to find the optimal placement of the waveguides and antennas to 1) maximize the so-called "tritium breeding ratio" or TBR defined as the number of tritons produced per source 14.1 MeV neutron and 2) minimize damage and activation to increase waveguide and antenna lifetime. This thesis will systematically and rigorously calculate the optimal location through the use of the Monte Carlo N-Particle (MCNP) transport code for a variety of blanket materials [12].

The thesis is organized as follows. A review of the ARC reactor, on which the MCNP model used in this thesis, is based is described in Chapter 2, along with materials for liquid and solid blankets and acceptable damage and TBR limits. The MCNP code and model used for the thesis is presented in Chapter 3. Some general results regarding tritium breeding and blanket design are shown in Chapter 4. The TBR and damage results of running MCNP for four different blanket materials are presented and interpreted in Chapter 5. The activation analysis for the vacuum vessel is described in Chapter 6. Conclusions and future work are outlined in Chapter 7.

Chapter 2

Review of fusion reactor designs

This chapter reviews information important for placing into context the technical analysis of this thesis. In Section 2.1 the ARC fusion pilot plant reactor design [1] is discussed, on which the MCNP model used for this thesis is based. In addition, several generic liquid and solid blanket design options are presented for an ARC-like device, which will be used to expand the scope of our analysis past the details of the ARC blanket choices. In Section 2.2, acceptable limits for neutron damage, as measured by displacements per atom (DPA) and volumetric helium production from neutron-induced transmutation, as well as the minimum tritium breeding ratio (TBR) necessary to sustain the reactor are reviewed.

2.1 The ARC reactor and blanket designs

2.1.1 The ARC reactor

A new design for fusion reactors has emerged in the past few years, proposed by Prof. Dennis Whyte, Plasma Science and Fusion Center research scientists, and students enrolled in the Spring 2012 Engineering Principles of Fusion Reactors design course. This design, the Affordable, Robust, Compact (ARC) reactor (Figure 2.1) was recently published [1], and is based on the guiding principle of minimizing size to reduce cost and development times. ARC's design inspiration comes from fission designs, where small, modular reactors could become the next generation fission plants. With a major radius of only 3.3 m and an electrical power output of 261 MW (fusion power is 525 MW), ARC qualifies as a small, modular fusion reactor. Its goal is

dual purpose: to serve as a Fusion Nuclear Science Facility to test the irradiation of components in a high-energy neutron and reactor-like environment, and to serve as the first demonstration fusion power plant. To reach the goal of being affordable, the design study sought a reduction in size. ARC accomplishes this reduction in size through several means, not least of which are the use of high-field-side RF launch and the immersion liquid blanket, which is made possible with demountable toroidal field magnets composed of newly-available high-temperature superconductors.

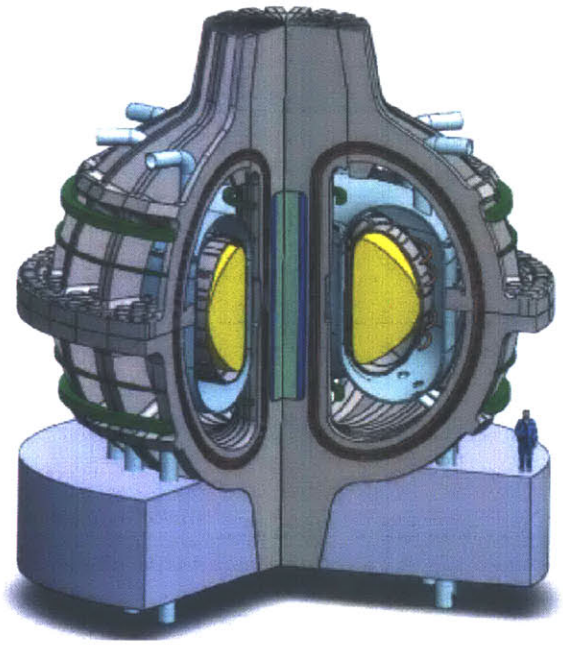

Figure 2.1. CAD model of the MIT ARC reactor, with a person shown for scale [1]. The plasma is in yellow with a tight-fitting vacuum vessel, immersion blanket tank, and connections in aqua, superconductor coils in brown, vertical field coils in green, and structural components in grey.

This thesis, in part, seeks to verify that the decision to employ high-field-side RF launch within an immersion blanket is not only beneficial for efficient RF current drive, but also for fuel breeding and radiation damage. As such, we have based our MCNP model on the original ARC MCNP model, which is shown in Figures 2.2 and 2.3.

Summarizing briefly, the vacuum vessel is broken up into two parts, moving outward in minor radius. The inner part, closest to the plasma, contains a plasma-facing wall composed of

~mm thick tungsten. ARC employs a double-walled vacuum vessel (VV) composed of Inconel 718, which is an alloy primarily composed of nickel, chromium, iron, and niobium (the exact composition is given in Appendix A). Enabled by the use of an immersion blanket, ARCs's vacuum vessel is cooled with FLiBe (the main breeding and moderating material) flowing through the double-walled VV. This choice greatly simplifies nuclear and plasma heat removal from the VV since the coolant is directly pumped from a large reservoir of FLiBe. The outer part of the vacuum vessel also has a non-structural beryllium layer for neutron multiplication. Surrounding the vacuum vessel is the FLiBe blanket, which is contained in the blanket tank, also composed of Inconel 718. The operating temperature of the FLiBe is roughly ~850-900 K. The outside the blanket tank has an insulating layer, which is cooled with water near room temperature. A dedicated neutron shield composed of titanium dihydride is used outside the blanket tank, which also operates at RT. Further insulating layers then follow and finally, for neutronics purposes, one arrives at the superconducting toroidal field magnets, which operate at 25 K with cryogenic cooling. The present neutronics design includes a simple open-ended thicker tungsten divertor (yellow in Figure 2.2) for concentrated heat removal and a physical support post (red) though which all connections pass.

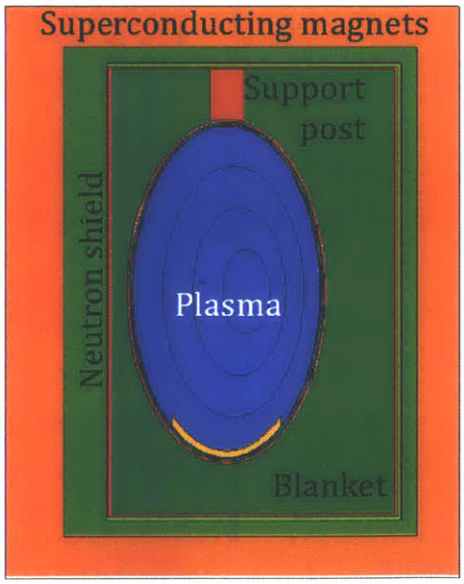

Figure 2.2. MCNP model of the ARC reactor [1]. The plasma is shown in blue and is surrounded by a multi-component vacuum vessel, which is suspended by a support column shown in red. The distance from the far left to the center of the plasma is 3.3 m (major radius), and one-half of

the midplane distance between ends of the vacuum vessel is 1.1 m (minor radius). Figure not to scale.

Inputs into the MCNP model and dimensions of the materials are included in Table 2.1. Note that the plasma is divided into four regions (nested toroids) to provide sufficient geometric accuracy for the 14.1 MeV neutron source.

Modifications to the ARC model for this study will be justified in the next two chapters, which include moving the major radius from 3.3 to 3.6 m and changing the elliptical vacuum vessel into a D-shaped one. Thicknesses for the vacuum vessel and outer components remain the same.

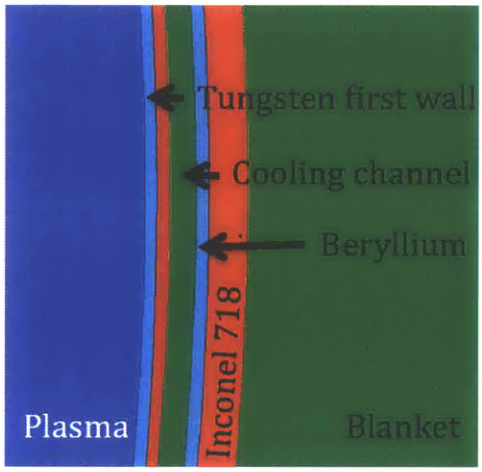

Figure 2.3. Zoom (1:4.72 scale) in of the outer midplane region of the vacuum vessel.

Region	Thickness/Length/Radius
Major radius of plasma	3.3 m
Plasma region 1	Centered at 3.53 m; z = 50 cm; x = 28
Plasma region 2	Centered at 3.45 m; z = 100 cm; x = 55 cm
Plasma region 3	Centered at 3.38 m; z = 150 cm; x = 83 cm
Plasma region 4	Centered at 3.3 m; z = 208; x = 181 cm
Plasma-facing first wall	1 cm radially thick
Inner vacuum vessel	1 cm radially thick
Cooling channel	2 cm radially thick
Be multiplier	1 cm radially thick
Outer vacuum vessel	3 cm radially thick
Blanket (at midplane)	Inboard: 20 cm thick; outboard: 80 cm thick
Blanket tank	3 cm thick
Thermal insulation	5 cm thick

Neutron Shield	50 cm thick
Vacuum gap	1 cm thick
Toroidal field coils	70 cm thick

Table 2.1. Thicknesses, lengths, and radii for each region in the full model used for this study. Plasma regions are ellipses; the lengths in z- and x- are given. Note that the blanket thickness is given for the midplane.

2.1.2 Blanket designs

Several components must be considered in a blanket design: the blanket material itself, the structural material containing the blanket, and the coolant. We will consider each of these components in turn, beginning with blanket materials. Proposed fusion blankets can either be liquid or solid. Some examples of liquid blankets include lithium, lead-lithium eutectic, and molten salts such as FLiBe used in ARC. Solid blankets include lithium ceramics [13].

Liquid blankets need to be pumped in and out of the device, and during maintenance need to be completely drained from the containing structure. Pumping allows for constant tritium recycling and recovery since it is dissolved in the liquid. They also require structural/vacuum-interfacing materials between them and the plasma (not just plasma-facing components), as liquids do not provide any structural support. Two major advantages of liquid blankets are 1) that damage rates are irrelevant for liquid blankets since DPA has no real meaning in a liquid, and 2) there is no risk to a liquid blanket from disruptions since the vacuum vessel would move within the liquid and the liquid will absorb some of the shock. Importantly, liquid blankets reside outside the vacuum vessel so they operate at atmospheric pressures.

Solid blankets, on the other hand, can provide some structural support, so they only require a plasma-facing first wall. However, we do care about neutron-induced damage rates to solid blankets since severe damage can degrade the structural integrity. Solid blankets must place the vacuum vessel on the outside, since the vacuum vessel (VV) must be a lifetime component; this forces solid blankets to also operate inside a vacuum. Solid blankets also risk damage from disruptions. Tritium recovery is obtained by circulating the breeder/coolant through the blanket, and can only be completed when the solid blanket is removed from the reactor during maintenance periods.

Structural materials include ferritic/martensitic steels that are low-activation such as F82H, vanadium alloys, and silicon carbide. Low activation, radiation resistant ferritic steels are considered to be good candidates due to low radiation swelling, a low thermal expansion coefficient, and a high resistance to creep [14, 15]. Silicon carbide is a ceramic that has low electrical conductivity and has been demonstrated computationally to work well with a lead-lithium blanket [16]. It does have some disadvantages, including difficulties manufacturing and a low outlet temperature leading to a low thermal efficiency [16]. Vanadium has also been considered due to its favorable activation properties but has disadvantages, including needing an insulating coating to lower conductivity and help with any effects on the MHD equilibrium in the plasma, as well as adverse reactions with lithium [14].

Possible coolants include water, helium gas, liquid lithium, and molten salts. A liquid blanket material can serve as the coolant for its structural material (e.g. ARC). Another advantage of using the blanket material as the coolant, as will be seen in Chapter 4, is that any amount of blanket close to the plasma will contribute to TBR than blanket further away, meaning that the coolant layer can substantially contribute to tritium breeding. Solid blankets will typically include either water or helium as the coolant.

To keep this study simple and compare only the performance of the waveguides and launchers, Inconel 718 is used as the main structural material. This still allows the use of a variety of blanket materials with corresponding coolants in the MCNP model.

2.2 Acceptable TBR and damage rates

2.2.1 Acceptable TBR

Referring to the previous chapter, each fusion reaction requires one deuteron and one triton in order to occur. Each neutron-lithium reaction produces one triton. At an absolute minimum, each neutron produced by the fusion reactions must react with lithium to produce a triton in order to have a sustainable fuel cycle. This gives a theoretical minimum TBR, defined as the total number of tritons produced per source neutron, of unity.

However, tritium can be unrecoverable from several different sources. First, as mentioned, tritium has a half-life of only 12.3 years, thus one is continuously losing tritium fuel at a small but significant rate and long-term (decadal) storage is not an option. For this reason fusion devices must continuously breed and recycle tritium. Second, some of the tritium produced may end up trapped in structural components and are not easily recoverable, especially if trapped in permanent structural components such as the blanket tank. And third, while some proposed tritium extraction methods predict recovering 99% of all tritium from a blanket, these methods are unverified [17, 18]. The literature has traditionally chosen a TBR of 1.1 as a reasonable target design to account for any losses listed above and also uncertainties in the cross-sections [19, 20], although values up to 1.2 have also been used as a target, to account for the necessity of using a FNSF to build up a tritium supply for DEMO [21, 22].

This study will not focus on overall TBR; instead, it will examine differences in TBR for different locations of waveguides and an antenna around the vacuum vessel. However, whether or not the blanket materials chosen meet the minimum acceptable TBR of 1.1 for a FNSF in the given blanket design will be reported.

2.2.2 Acceptable damage and activation rates

As we will consider damage to the waveguides and antenna in Chapter 5 and activation in Chapter 6, we will discuss acceptable damage and activation rates, specifically for structural materials relevant to our MCNP model.

The present model uses Inconel 718, which has not yet been tested for irradiation studies. However, ferritic steels have an estimated irradiation lifetime of 150-200 DPA [14], and martensitic steels show some gains in yield strength and decreases in ductility at a helium concentration of 500 atomic parts per million (appm) [23, 24]. Inconel is expected to have similar but lower irradiation limits, because it is not tailored for the hard fusion neutron spectrum. In general, for FNSF studies it is considered feasible that most high-strength steels can be estimated to degrade significantly in excess of 20-25 DPA [25], but that after these levels the response of steels in complex fusion components is unknown, mostly due to the elevated helium production rate caused by the high-energy fusion neutrons. Indeed this unknown behavior of

structural components at greater than 25 DPA is the primary motivation for designing a FNSF which would provide large fluence testing of components in a fusion neutron spectrum.

In terms of activity, dose rates in Inconel 718 are expected to be primarily from Ta-182, Mn-56, Co-58, and Ni-57 [26]. Since our model is based on the ARC reactor that has a fusion power output of 525 MW, this means that 1.86×10^{20} neutrons/sec are expected to be released in the model reactor. Recent activation calculations were performed for predicted performance of the JET fusion device in England, assuming 2×10^{19} neutrons/day of irradiation or 2.3×10^{14} neutrons/sec. JET is a good comparison device since it is roughly the size of ARC. For the JET design, the total dose rate in Inconel 718 at shutdown is 295 mSv/hr (total contact dose rate), almost 43% of which is due to Ta-182, and roughly 20 mSv/hr one year after shutdown [26]. These dose rates classify as high-level waste [27], and the dose limit for a worst-case accident is 10 mSv [28] if no evacuation is required. ARC and this study's model are expected to have much larger dose rates due to the larger neutron fluence.

Chapter 3

Neutronics and the 2-D MCNP model

This chapter gives a more complete description of the 2-D MCNP neutronics model used for this study. In Section 3.1, the underlying equations used to calculate the TBR, DPA, and He retention, as well as a brief description of the Monte Carlo method are discussed. In Section 3.2, the waveguide and antenna design for the 2-D MCNP model is discussed. In Section 3.3, the MCNP models used for this study are presented. And finally, in Section 3.4, the test setup including the specific materials and antenna locations chosen is described.

3.1 Introduction to underlying theory behind MCNP

The Monte Carlo Neutral Particle transport code [12], MCNP, was used to obtain the results in this thesis. It solves the neutron transport equation by calculating the trajectories and interactions of individual neutrons [29]. The user first defines a source of neutrons which are to be "tracked". For our purposes, we can define a source by making predictions inside a model plasma of the number of neutrons being produced every second; our model will include a plasma temperature and density profile to determine the reaction rate. The neutrons are then tracked as they move leave the plasma, and move through the first wall, vacuum vessel, blanket, and beyond. Their interactions (scattering, absorption, leakage) with the different atoms that make up these regions are recorded and tallied [29]. With sufficient tallies, i.e. Monte Carlo "counts" of particular interactions, a statistically meaningful result is obtained that reflects the expected ensemble behavior of the highly-penetrating neutral particles (neutrons, gammas) resulting from the original neutron source.

All three quantities of interest are considered to be flux tallies measured in terms of the source neutrons, specifically looking at the flux within a cell. A cell is simply a defined spatial region within the MCNP input; the components of the vacuum vessel, for example, are each cells. The general definition of volume-averaged flux is [29]:

$$\overline{\phi_V} = \frac{1}{V}\int dV \int dE \int dt \int d\Omega\, \psi(\vec{r}, \hat{\Omega}, E, t), \tag{3.1}$$

where E is the energy, t is time, V is volume, Ω is solid angle, and ψ is the angular flux. For our purposes, the source neutrons are monoenergetic, so E is exactly 14.1 MeV for the neutrons entering the vacuum vessel; they will be moderated as they collide and interact with atoms in the vessel. We also assume that the reactor we are modeling is in steady state - that is the rate of fusion reactions is constant. This implies no need to integrate over time. We can simply multiply by the length of time in seconds to obtain any quantities needed. Typically we consider time in Full Power Years (FPY). Ψ is defined as the particle density, n, multiplied by the particle speed. Thus the volume-averaged flux has units of particles per cm^2 per source neutron.

We can now consider each quantity. We begin with tritium breeding ratio (TBR), which is defined as the number of tritons bred per source neutron. Again, assuming a steady state reactor, this is not a function of time. MCNP calculates TBR by calculating the neutron flux defined above and counting how many neutrons react with lithium in the cooling channel and the blanket to produce tritium.

Next is the volumetric helium production/retention, which is defined in a similar manner. MCNP calculates the neutron flux and instead of counting the number of tritium-breeding reactions, it counts the number of helium-breeding reactions produced through the (n,α) transmutation reactions. Note that the helium is assumed to be "retained" at the location where it is born due to its very short range in solid materials. The structure of the input in MCNP is exactly the same. If we wish to compute the He retention after one FPY, we need to multiply the MCNP output by the number of source neutrons output per year and divide by the number of atoms in the specific region of interest, weighting the result to obtain atomic parts per million (appm), which is the standard metric to gauge material changed due to volumetric helium retention. This is a called a tally multiplier. The formulas are given below:

$$\#\ source\ neutrons = \frac{P_f(365*24*60*60)}{17.6\ \text{MeV}*1.602\text{e}^{-19}}, \tag{3.2}$$

where P_f is the fusion power. This gives the He retention:

$$He\ (appm) = \frac{\text{MCNP output}*\text{\# source neutrons}}{10^6*\text{\# atoms in region}}. \tag{3.3}$$

Finally, we consider the displacements per atom, or DPA. Again, the calculation begins as a flux tally and counts the number of displacement interactions. However, these displacements will not take place unless the colliding neutron has at least the displacement energy, E_d. The cross sections must be tallied over a DPA-weighted material, rather than the original material input. The process for weighting the material cards is explained in [30]. The tally multipier is given below:

$$DPA = \frac{(MCNP\ output)*\#\ source\ neutrons*\rho'_{tot}}{\rho_{tot}}, \tag{3.4}$$

where

$$\rho_{tot} = \sum_{i=1}^{N} \rho_i\,,\ \rho'_{tot} = \sum_{i=1}^{N} \rho'_i, \tag{3.5}$$

is the summation of all isotopes, primed and unprimed, and where

$$\rho'_i = \rho_i \frac{E_{d,ref}}{E_{d,i}} \tag{3.6}$$

is the DPA-weighted density of isotope i, and $E_{d,ref}$ is the reference displacement energy and $E_{d,i}$ is displacement energy of isotope i. The DPA weighting comes out of the fact that MCNP computes DPA with a DPA response cross section, which is a function of the displacement energy. After writing the DPA response cross section in terms of the displacement energy, the density of atoms can be divided by the displacement energy to yield a DPA-weighted density. The reader is referred to [29] for more details about this.

3.2 MCNP waveguide and antenna design

As mentioned above, we have employed the two-dimensional version of MCNP to perform this study. As such, the waveguides and antennas are toroidally continuous, i.e. the 2-D nature of the calculation arises from a simplying assumption of toroidal symmetry, which to first order is well-justified in a tokamak. In a real device, they would have finite height and width and would not extend all the way around toroidally; this would be possible in a three-dimensional MCNP model and is left for future work to be discussed in Chapter 7.

The size of the waveguides is determined by the frequencies of the RF waves to propagate in them. For some a waveguide of some dimensions, there exists of cutoff frequency below which the wave will not propagate: the smaller the waveguides, the higher the cutoff frequency. As mentioned in Chapter 1, the LH frequencies are in the GHz range, while ICRF are in the tens of MHz. The model is based on the LH waveguides, which for a few GHz yield waveguides around 5 cm in width [31]. The height and the width of the launcher/antenna are determined by the current drive efficiency equation given in Chapter 1. Since a tokamak will have a defined major radius, as well as an operating point for the density and the current, this leaves two undetermined variables: the efficiency itself and the power absorbed. A reasonable value for the efficiency can be chosen based on values already achieved, say $\eta = 0.3 \times 10^{20}$ A/W/m^2 [4]. A more conservative value of 0.23×10^{20} was chosen, which provides a realistic upper limit to the physical size of the launching structures. For an ARC-sized device, this gives a required absorbed power of 60 MW, which is the value chosen for this study. Note that the design value for ARC is ~38 MW due to higher calculated CD efficiency using high-field launch. To be conservative and account for long pulses and passive waveguides, as well as degradation over time, a large launcher area should be chosen. About 5 m^2 was assumed to be the total desired surface area [4], thus giving a conservative 12 MW/m^2 average launcher power density. For a toroidally continuous waveguide and antenna in which the width is just the circumference of the torus, this gives an antenna poloidal height of 30 cm at the inboard midplane ($R \sim 2$ m), and 15 cm at the outboard midplane ($R \sim 4$ m).

The components of the waveguides and the antenna include a metal structural material with some transmission coating to increase electrical conductivity and thus provide efficient RF transmission. Several materials can be used, namely low-activation ferritic steel for the metal structure and either molybdenum or tungsten for the transmission coating. In this study, we chose molybdenum for the coating, but Inconel 718 for the structural material since it was chosen as the structural material for the vacuum vessel and blanket tank in ARC. The activation of Inconel 718 will be discussed further in Chapter 6. The transmission coating, which only has to be a thickness corresponding to several skin depths, is only about 1% of the total volume of the waveguides, with the rest of the volume being split evenly between structural material and the vacuum in which the RF propagates. In the MCNP model, rather than splitting the waveguides into regions of structure and vacuum, a region of only Inconel structure was used but at half the

normal density to give an average assessment of the DPA and helium retention. Since the average spatial dimension of the waveguide structures is on the order of centimeters and the neutron mean free path is roughly 10 cm, this simplification will not affect the accuracy of the simulation.

In conventional designs, the waveguides are placed at the outboard midplane and come straight into the device horizontally. This lets free-streaming neutrons through the waveguides in the vacuum region. In a reactor, this leads to unacceptable degradation of the superconducting toroidal field magnets at the outboard midplane. To mitigate this, the waveguides have to be installed with bends (or chevrons) so that they are not straight everywhere. One way to accomplish this is to bend them at right angles, as shown in Figure 3.1 below.

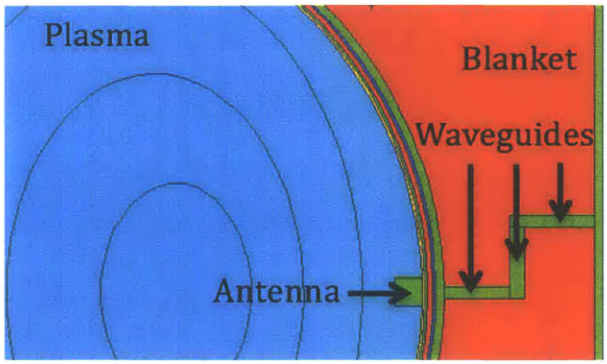

Figure 3.1: Outboard midplane waveguide (shown in green) which is bent at right angles to prevent free-streaming neutrons from reaching the toroidal field magnets, and for the purposes of constructing the MCNP model, is comprised of three different sections.

In keeping with waveguides coming in to the vacuum vessel from the top of the tokamak, as in ARC, another configuration is to have the guides come straight down and then bend into place at an angle. This is shown below in Figure 3.2.

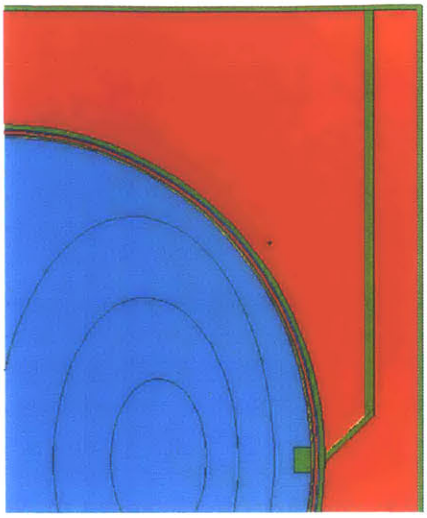

Figure 3.2. Alternative design for waveguide design for outer midplane launch (shown in green), in which they come from the top of the blanket tank and bend at an angle into the appropriate location.

The second design used to obtain most of the results in the thesis, but a scenario with the first design was run to make a formal comparison. The comparison will be presented in Chapter 5. A summary of all waveguide and antenna properties used for this study is given in Table 3.1.

Property	**Value**
Waveguide/antenna structure material	Inconel 718
Transmission coating	Molybdenum
Density of structural material	4.1 g/cm^3
Waveguide width	5 cm
Transmission coating thickness	1 mm
Transmission coating density	10.28 g/cm^3
Total absorbed power in plasma	60 MW
Total surface area of antenna	4.8 m^2
Antenna radial build	10 cm

Table 3.1: Properties and inputs of the waveguide and antenna designed used for MCNP.

3.3 MCNP models used for this thesis

The model of the ARC device was briefly described in Chapter 2. The two MCNP models used in this thesis are based heavily on the ARC model and are described in full detail in this section. The first "full" model includes every region in the ARC model, including insulation and the toroidal field magnets. The second reduced or "stripped" model, the one used for almost all tests, has the exact same dimensions as the first, but does not include anything radially beyond the blanket tank since the primary focus of this study is the effect on TBR and internal damage rates. In fact, an initial comparison between results from the full model and the stripped model revealed little differences for the DPA and helium production in the vacuum vessel as well as TBR in the cooling channel and blanket tank.

The original ARC model used a simplified elliptical vacuum vessel. This has been replaced in our new model with a more realistic D-shaped vacuum vessel, as shown in Figure 3.3 for the stripped model, which provides a tighter fit to the plasma shape.

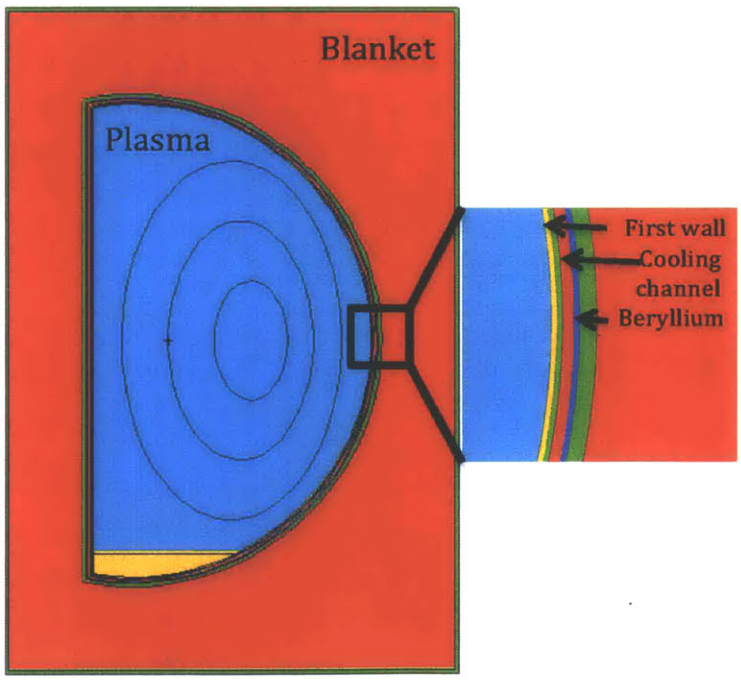

Figure 3.3. Stripped model with D-shaped vacuum vessel. Inset shows components of the vacuum vessel. Sky blue: plasma; orange: tungsten first wall and divertor at bottom of vessel;

green: Inconel vacuum vessel; red: cooling channel and blanket (in this case, the blanket is liquid FLiBe); dark blue: beryllium layer. The ellipses in the plasma represent flux surfaces used to define the neutron source in MCNP. The major radius (distance from center of tokamak to the center of the plasma) is 3.6 m, in part due to the Shafranov shift of the plasma towards the outboard side (as can be seen by the plasma contours) and due to increasing the major radius from 3.3 m to optimize the inboard blanket thickness.

This is desirable here because the launcher structures located at the VV/first wall will be in close proximity to the boundary plasma and this better captures the requirement of the launchers to couple their power through the boundary (again, vacuum propagation is not possible for LH and ICRF frequencies). The D-shape consists of elliptical surfaces on the outboard side with straight vertical edges on the inboard side. The radial thicknesses of the components are the same as in the ARC model and are given in Table 3.2. For details regarding the components outside the blanket tank, the reader is referred to Chapter 2. The MCNP cell and surface cards are given in the Appendix A.

Region	**Thickness/Length/Radius**
Major radius	3.6 m
Plasma region 1	Centered at 3.75 m; z = 50 cm; x = 28
Plasma region 2	Centered at 3.76 m; z = 100 cm; x = 55 cm
Plasma region 3	Centered at 3.6 m; z = 150 cm; x = 83 cm
Plasma region 4	Centered at 3.6 m; z = 208; x = 181 cm
First wall	1 cm thick
Inner vacuum vessel	1 cm thick
Cooling channel	2 cm thick
Be multiplier	1 cm thick
Outer vacuum vessel	3 cm thick
Blanket (at midplane)	Inboard: 45 cm thick; outboard: 55 cm thick
Blanket tank	3 cm thick
Thermal insulation	5 cm thick
Neutron Shield	50 cm thick
Vacuum gap	1 cm thick
Toroidal field coils	70 cm thick

Table 3.2. Radial thicknesses, poloidal lengths, and major radii for each region in the full MCNP model used for this study. Plasma regions are ellipses; the lengths in *z*- and *x*- are given. The stripped model includes all components except those outside the blanket tank.

3.4 Test setup with materials and location choices

Four different blanket materials were chosen for this study: two liquid blankets and two solid blankets that have been proposed in the literature as possible blanket candidates, including FLiBe which was chosen as the blanket material for ARC. They are listed in Table 3.3, with some physical properties that were used in the MCNP input files. Four blankets were selected to test whether the results regarding the dependence of launcher location are material-dependent due to differences in neutron transport. Since the ARC study found that lithium enriched with 90% lithium-6 gave the best TBR results, we used 90%-enriched lithium for all blankets. The liquid blanket materials also served as the coolant in the cooling channel in the case of liquid blankets. For solid blankets, helium gas at a density of ~0.005 g/cm^3 serves as the coolant for the solid blanket and VV/first wall which is consistent with the favored dual-coolant Li/He design for solid blankets.

Material	Composition (atomic)	Density (g/cm$^{3)}$	Phase	Ref.
FLiBe	57.1% Fluorine 14.3% Beryllium 25.7% Li-6 2.9% Li-7	1.973	Liquid eutectic	[32]
Pb-17Li	83% natural Pb 15.3% Li-6 1.7% Li-7	9.55	liquid	[32, 33]
Li_4SiO_4	47.6% Oxygen 4.8% Silicon 42.8% Li-6 4.8% Li-7	2.39	solid	[34-37]
Li_2TiO_3	16.7% natural Ti 50% Oxygen 30% Li-6 3.3% Li-7	3.43	solid	[38]

Table 3.3: Physical and material properties for the four simplified blankets used for this study, with density, temperature, phase and structure. All materials used a 90% lithium-6 enrichment.

The general setup for testing included computing the TBR, DPA, and He retention for all four blankets in seven different poloidal locations for the RF launchers. Each MCNP run would be for

one blanket material and one location at a time, for a total of 28 different scenarios and 84 different quantities measured. The launcher locations include the inboard and outboard midplane, directly above the vacuum vessel, the inboard and outboard corners, and inboard and outboard between the midplane and the corners. Poloidal angles of the launchers are shown in Figure 3.4.

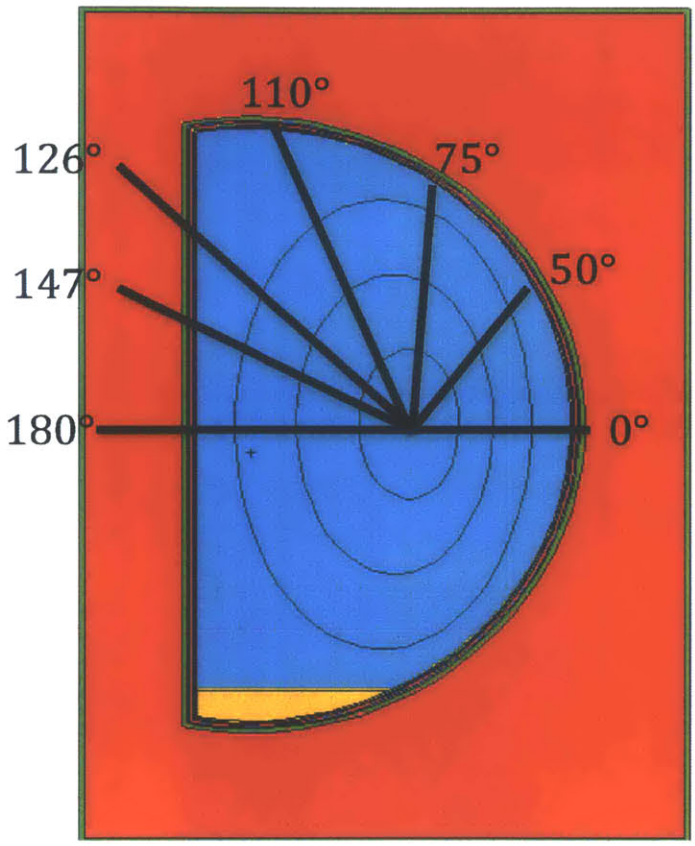

Figure 3.4. Poloidal angles of the seven test locations where the RF- antennas/launchers were placed in the MCNP simulations. They include the inboard (180°) and outboard (0°) midplane, top of the vacuum vessel (110°), inboard (126°) and outboard corners (75°), and in between the midplane and corners on both the inboard (147°) and outboard (50°) sides.

Only locations at or above the midplane were chosen the MCNP model is based off of the ARC design, which has the waveguides coming in from the top in a plug-and-play immersion blanket scenario. Regardless one expects a high degree of up-down symmetry in this study.

Chapter 4

Blanket design considerations

In this chapter, a better sense of how certain properties of blankets designs affect tritium breeding will be gained. In Section 4.1, how blanket thickness impacts TBR is considered. In Section 4.2, the affects of adding a neutron multiplier to the blanket are discussed. In Section 4.3, the results of varying placement of the vacuum vessel in a fixed blanket tank are presented.

4.1 Blanket thickness

Recall from Chapter 1 the three purposes of the blanket: 1) to breed tritium in a closed fuel cycle, 2) to moderate neutrons to prevent radiation damage to the toroidal field magnets, and 3) to transfer heat from neutrons to blanket so that it can be extracted and used to generate electricity. In general, the thicker the blanket, the more tritium that is bred, the lesser the damage to the magnets, and the more heat that is deposited for energy extraction. However, a reactor must have a finite-sized blanket since too much volume substantially increases reactor cost [39]. We must find a thickness of the blanket that reasonably accomplishes these three tasks without adding too much volume to the device.

Of this thesis' three goals, this thesis will focus on the first issue of breeding which typically has the least margin of error. This is because while the blanket can moderate neutrons for radiation damage prevention, a neutron shield and reflector outside the blanket to capture and reflect the neutrons that escape the blanket can also be used. Some proposed neutron shields include zirconium dihydride and titanium dihydride, the latter included in the ARC design [1, 40]

Preliminary neutronics work reveals that most breeding takes place within 0.5 m of blanket, measured as the distance from the edge of the plasma outward. The recent Vulcan star

study calculated TBR vs. blanket thickness with MCNP for a variety of proposed blanket materials (Figure 4.1) [41]. The study assumed a one-inch-thick Inconel 625 vacuum vessel with a 2 mm tungsten first wall (similar to the ARC design). As shown in the figure, most of the increase in TBR takes place within the first 40 cm of blanket for most materials. By 70 cm, the TBR has plateaued for those same materials [41]. The reason for this is complex but can be primarily attributed to the average location where thermalization of the neutron occurs. This is evident by the fact that pure low-Z blankets (e.g. LiD), being more efficient at moderation, have their TBR plateau at smaller distances than blankets with high-Z materials (Li-Pb).

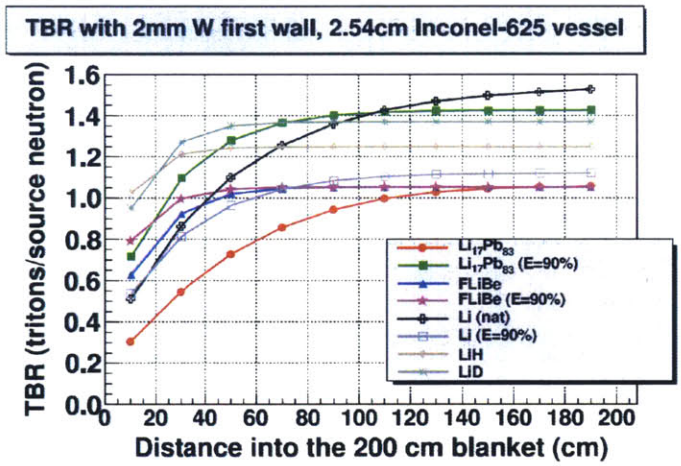

Figure 4.1. TBR vs. distance into blanket (cm) for various proposed blanket materials [40]. Note that most of the increase in TBR occurs within the first 40 cm of material and the TBR maximizes at about 70 cm, for most proposed blankets.

However these calculations did not account for the necessary cooling channel within the vacuum vessel. Extending the idea above, however, a series of MCNP runs was completed in which the thickness of the cooling channel was varied, while the size of the blanket tank remained constant (thus the outer blanket volume decreased). A one cm thick tungsten first wall with a one cm thick Inconel 718 vacuum vessel was assumed and were fixed. The beryllium and outer vacuum vessel thickness are one cm and three cm, respectively, and moved further out in the minor radial direction as the cooling channel thickness increased. The test was completed for FLiBe only (Figure 4.2). From the figure, the thinner the initial structure between the plasma and

the blanket, the higher the TBR, regardless of the volume of the outer blanket. It is better to have the blanket material as close to the plasma as possible.

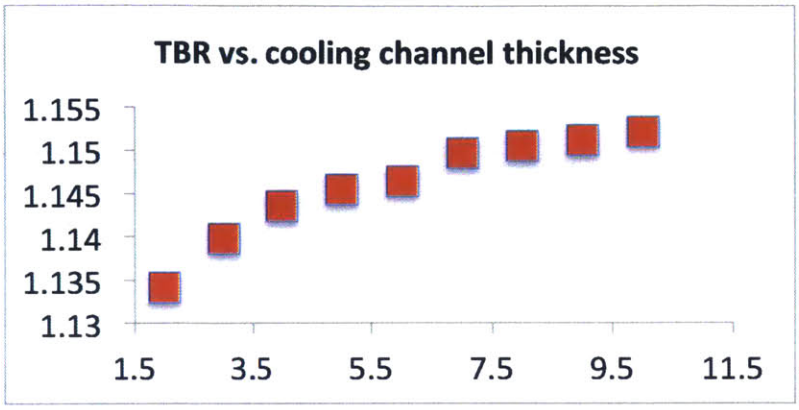

Figure 4.2. TBR vs. thickness of cooling channel (cm). Keeping the first wall and inner vacuum vessel in place, the cooling channel thickness was incrementally increased from 2 cm up to 10 cm, while keeping the total volume of the blanket tank constant (thus the thickness of the outer blanket decreased). Thickness of all other vacuum vessel components remained the same as mentioned in Chapter 3. The original ARC model was used to generate the data for this figure, without the divertor.

4.2 Effect of neutron multiplier

A neutron multiplier, such as beryllium, zirconium, and lead, can have nuclear reactions with a neutron that produce more than one neutron, thus multiplying the neutron flux. The (n,2n) reaction for beryllium is attractive due to its low activation energy and is given below; it requires neutrons of at least 1.9 MeV, which is easily satisfied by fast fusion neutrons before thermalization [42]:

$$^{9}_{4}\mathrm{Be} + \mathrm{n} \rightarrow 2(^{4}_{2}\mathrm{He}) + 2\mathrm{n}. \quad (4.1)$$

A simple test was performed to demonstrate the effects of 1) not having a neutron multiplier, and 2) adding extra neutron multiplier to the cooling channel. For both cases, the original ARC model was used, without the divertor, with FLiBe as the blanket and cooling

material. In the first case, replacing the Be layer with FLibe resulted in a ~13% reduction to 0.98 in TBR compared to the original value of 1.134 shown in Figure 4.3 at the original cooling channel thickness. In the second case, adding an extra cm of Be (while keeping the cooling channel thickness constant) increased TBR by 5% to ~1.19 compared to the original value at the original cooling channel and beryllium layer thicknesses. The neutron multiplier is important to include early in the blanket not only for the increase in TBR, but because they are more effective when the neutron spectrum is hardest.

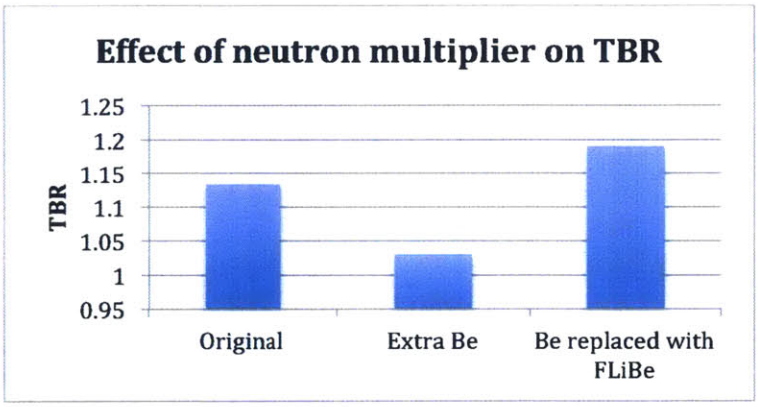

Figure 4.3. Bar graph illustrating the effects of removing the beryllium multiplier from between the cooling channel (FLiBe) and the outer vacuum vessel and replacing with FLiBe, and adding an additional cm of beryllium between the coolant and the outer vacuum vessel. In the former case, the removal resulted in a ~13% reduction in TBR, while in the later case, the additional beryllium increased TBR by ~5%.

4.3 Placement of vacuum vessel

As mentioned above, reactor cost depends heavily on the volume of the reactor core. A smaller major radius, at fixed aspect ratio, ensures that the volume and cost stay low. This implies that the thickness of the blanket on the inboard side must be as small as possible to minimize the major radius, while increasing the blanket thickness on the outboard side to maintain an acceptable TBR.

This creates an asymmetric blanket in the radial build. This is somewhat mitigated by the fact that the neutrons are also released from the plasma in a radially asymmetric manner, namely the Shafranov shift moves the center of the plasma closer to the outboard side. Nonetheless, it is important to consider the consequences of an asymmetric blanket. To do this, a series of MCNP runs was performed, varying the inboard (and outboard) thickness by moving the vacuum vessel outward in relation to the blanket tank (by incrementally increasing the major radius), which was of constant volume. A similar stripped model to the one presented in Chapter 3 was used for this set of runs with a FLiBe, with a starting inboard thickness of 20 cm at the midplane and a starting outboard thickness of 80 cm. The results are given in Figure 4.4. As can be seen, the TBR was maximized for an inboard thickness of 45 cm, or an outboard thickness of 55 cm, both at the midplane. This optimal thickness was chosen for use in all later runs, and the models presented in Chapter 3 reflect that choice. This sets the major radius to 3.6 m. However, in general one can see that a variety of inboard vs. outboard thickness provide viable TBR since the maximum is quite broad vs. inner blanket thickness.

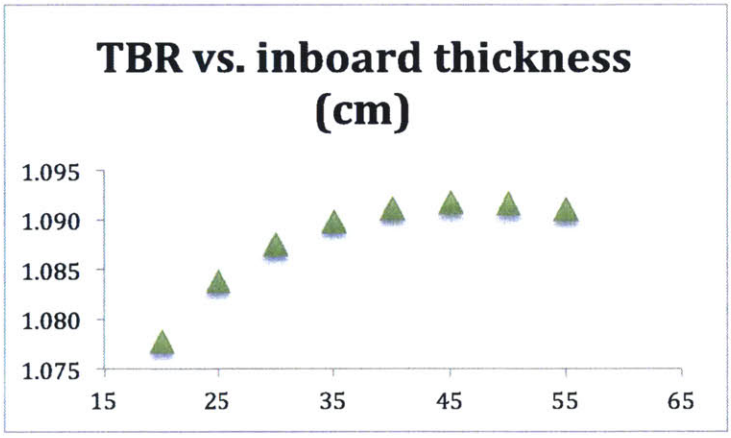

Figure 4.4. TBR vs. Inboard thickness of the blanket at the midplane. The stripped model was used for this set of runs, with the inboard thickness being varied from 20 cm to 55 cm (and the outboard thickness being varied from 80 cm to 45 cm), while keeping the tank volume constant, and thus the total thickness capped at 100 cm. The major radius was increased in increments of 5 cm. A midplane inboard thickness of 45 cm and a midplane outboard thickness of 55 cm gave the maximum TBR.

Chapter 5

TBR, DPA, and helium retention results from MCNP

In this chapter, the TBR, DPA, and helium production results are discussed. In Section 5.1, example MCNP output for a single location, as well as all seven, is provided for a single blanket material. In Section 7.2, overall results for all four blanket materials are presented. In the Section 7.3, results for the two waveguide designs are shown.

5.1 Example MCNP output

Following the test methodology given in Chapter 3, we provide some sample MCNP output for an enriched Li_4SiO_4 blanket run in Table 5.1, for a launcher poloidal angle of 147°. All tallies have been computed either directly from MCNP or using the equations in Section 3.1. For this case, the total TBR was 0.992, with tritium produced in two locations: the blanket and beryllium multiplier (there is a finite T-production cross-section in beryllium); the helium coolant does not contribute to the TBR. Note that the DPA and helium concentration are not reported for the coolant since the coolant is a single element, itself helium. The values listed in the table are for one FPY and are hence listed as a DPA rate, and are for the entire cells, rather than at specific locations within a cell (see Appendix A for the cell definitions). There can be differences of up to 10% on the inboard side vs. the outboard side for DPA and He concentration. See Appendix B for TBR, DPA, and He concentration for all locations and all four blankets materials.

Region	TBR	DPA/yr	He concentration (appm)
First Wall	0	11.45	2.64

Inner vacuum vessel	0	33.84	185.65
Cooling channel	0	-	-
Beryllium multiplier	0.0022	-	3160
Outer vacuum vessel	0	22.61	113.86
Blanket	0.9895	-	2540
Waveguides	0	3.61	2.55
Antenna	0	35.84	190.12
Blanket tank	0	0.0061	0.0160

Table 5.1. Sample MCNP output for the stripped model at with liquid enriched Li_4SiO_4 as the blanket material, and helium gas as the coolant for one FPY, at 147°. DPA/yr and helium concentration are not reported for the coolant and blanket layers, and DPA is not reported for the beryllium layer. Total TBR is 0.992.

Some results to note immediately are that, in general, DPA and helium concentration decrease moving radially outward from the plasma. This result is reasonable since the neutron flux decreases exponentially moving outward. The tungsten first wall is resistant to damage because it has a relatively smaller displacement cross section at 14.1 MeV compared to the atoms in Inconel 718, explaining the relatively low value for DPA [43]. The antenna DPA rate is large since it is placed inside the vacuum vessel. Note that due to needing a large number of particles to satisfy statistical checks, the tallies for the antenna and the waveguides only include the Inconel 718 portion, and do not include the molybdenum coating. Given the coating's thickness is only one mm comprising 1% of the launcher's volume, the molybdenum would likely not contribute much to the tallies. The Li_4SiO_4 blanket appears to be effective in moderating and absorbing neutrons since the DPA rate and helium concentration are much lower in the blanket tank than in the other components.

Example results for the optimal launcher locations for one blanket are also provided, specifically the enriched Li_4SiO_4 solid blanket with helium cooling layer. Figures 5.1 through 5.5. show the three tally values vs. launcher poloidal angle for the seven locations shown in Figure 3.4. The TBR is maximized when the waveguides and antenna were placed at the top of the vacuum vessel. This is expected since the least amount of blanket material was displaced by the waveguides in this location. What is striking is that the differences between the seven TBRs are all less than 1%, so little TBR is lost by placing the launchers elsewhere. All other tallies are maximized in either the inboard or the outboard upper corners. The corner locations bring the waveguides and the antennas away from the neutron-producing plasma as much as possible but

still allow propagation of the RF waves. The DPA rate in the antenna, and both helium concentrations in the antenna and waveguide are minimized in inboard corner; this can be explained by recalling that the Shafranov shift in the plasma moves the plasma toward the outboard side, so more neutrons are seen by the outboard side than inboard side. The DPA rate in the waveguide is minimized for the outboard corner, rather than the inboard corner. Referring back to Figure 3.3, we can see that there is significantly more blanket in the outboard corner than in the inboard corner. Thus any neutrons entering the waveguides in the outboard corner have been well-moderated compared to ones in the inboard corner, causing fewer displacements. The helium concentrations are not affected by this since the cross sections for the helium-producing reactions in Inconel 718 do not depend on neutron moderation.

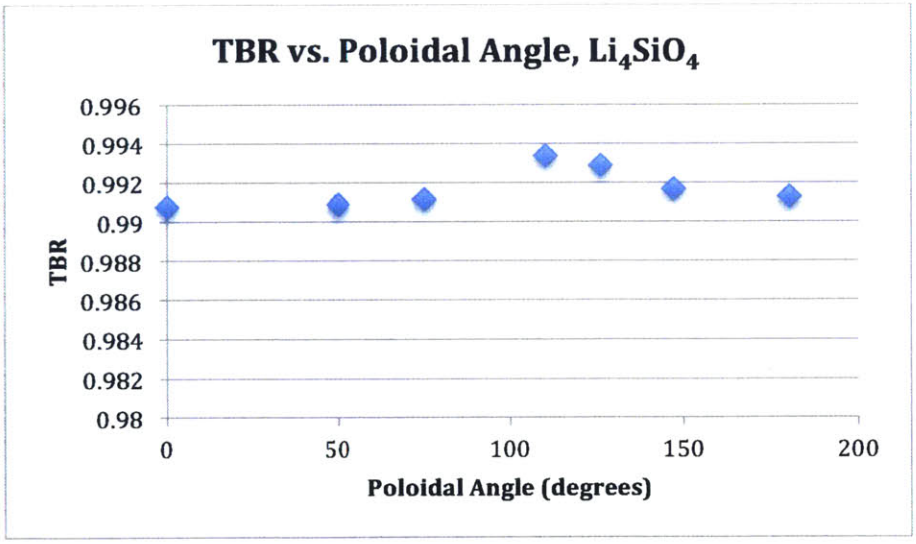

Figure 5.1. Total TBR in Li_4SiO_4 vs. poloidal angle. The peak TBR occurs at a poloidal angle of about 105°, or directly above the vacuum vessel towards the inboard side.

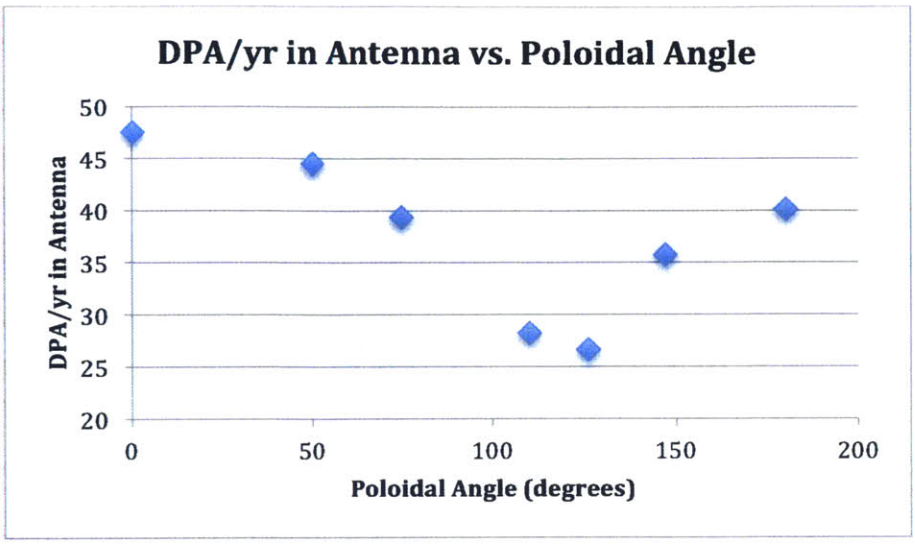

Figure 5.2. DPA rate in the antenna in Li_4SiO_4 vs. poloidal angle. The DPA is minimized at an angle of about 126°, or the inboard corner of the vacuum vessel.

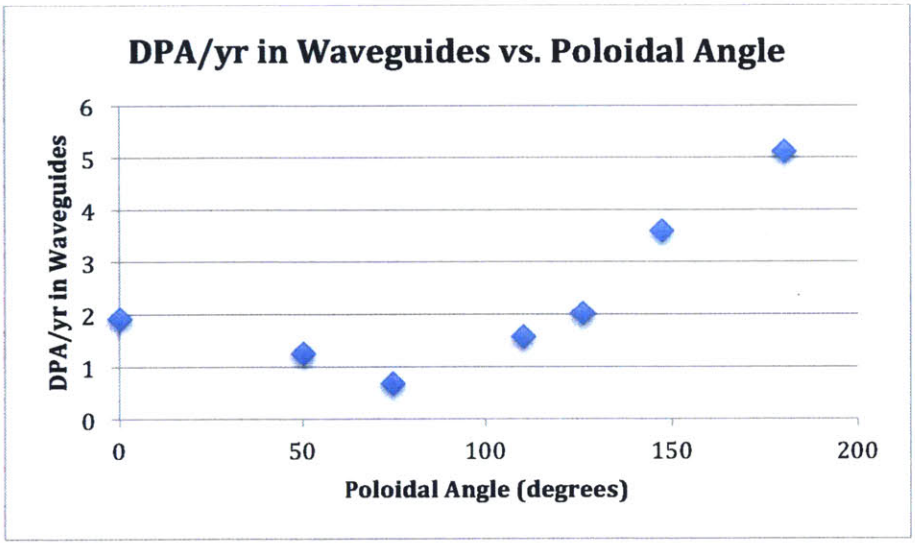

Figure 5.3. DPA rate in the waveguide in Li_4SiO_4 vs. poloidal angle. The DPA in the waveguide is minimized at about 87°, or in the outboard corner.

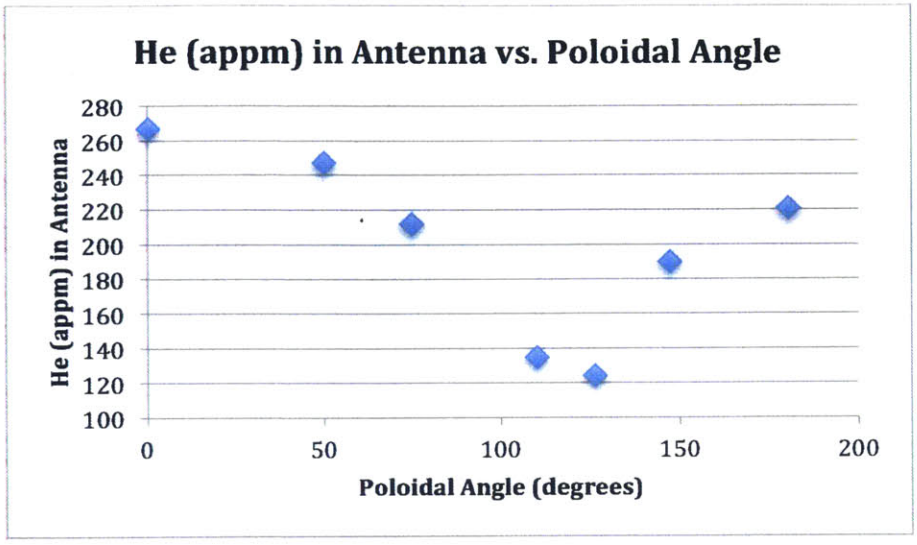

Figure 5.4. Helium concentration (appm) in the antenna in Li_4SiO_4 vs. poloidal angle. The helium concentration is minimized at about 126°, or in the inboard corner.

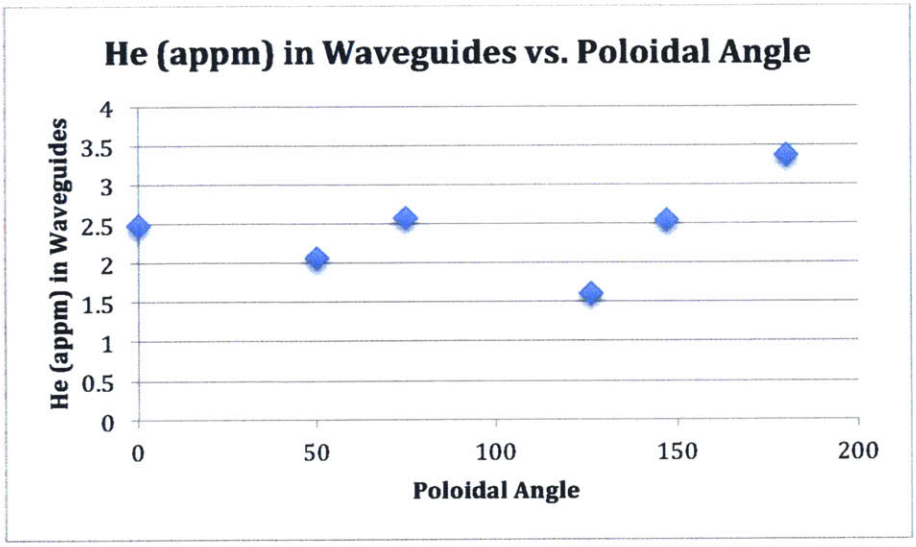

Figure 5.5. Helium concentration (appm) in the waveguide in Li_4SiO_4 vs. poloidal angle. The helium concentration is minimized for at about 126°, or in the inboard corner.

5.2 Overall results of scoping study on launcher poloidal location

Complete results for all locations and the plots for optimal locations for the other blanket materials are given in Appendix 2. In this section, we summarize the overall results for all four blanket choices and all poloidal launcher locations.

Table 5.2 summarizes the qualitative descriptions of the optimal locations for each blanket. For almost all quantities, all four blankets had the same optimal locations, meaning the results are independent of the blanket being in solid phase or liquid phase. The only real discrepancy is in the helium concentration for the waveguide, where three of the four blankets had optimal results in the inboard corner, and only enriched FLiBe had optimal results in the outboard corner. The liquid blankets saw their TBR maximized at either the top of the vessel or in the inboard corner. The solid blankets saw their TBR maximized at the top of the vessel, although differences in TBR between the top and the inboard corner (and the other locations) were small, generally less than 1%.

Blanket	**Total TBR**	**DPA/yr in waveguide**	**He (appm) in waveguide**	**DPA/yr in antenna**	**He (appm) in antenna**
FLiBe	Top / Inboard corner	Outboard corner	Inboard corner	Inboard corner	Inboard corner
Pb-17Li	Top / Inboard corner	Outboard corner	Inboard corner	Inboard corner	Inboard corner
Li_4SiO_4	Top	Outboard corner	Inboard corner	Inboard corner	Inboard corner
Li_2TiO_3	Top	Inboard corner	Inboard corner	Inboard corner	Inboard corner

Table 5.2. Summary of qualitative descriptions for the optimal locations for TBR, DPA rate, and helium concentration in all four blankets. They are essentially in agreement, meaning that there is no dependence on blanket phase material in determining the optimal location of waveguides and antennas.

Table 5.3. summarizes the quantitative optimal results for each quantity and each blanket. The TBR is higher in the liquid blankets because the blanket material is also used as the coolant, while helium gas (which has no reactions with neutrons to produce tritium) is used as the coolant for the solid blankets. The DPAs (for one FPY) are all comparable: within a factor of three for

the DPA rate in the waveguides, but small in absolute terms, and within 10% for the DPA in the antennas. DPA damage is noticeably higher in the Pb-17Li case due to its poorer moderation.

Blanket	Total TBR	DPA/yr, waveguide	DPA/yr, antenna
FLiBe	1.9024	0.73	25.91
Pb-17Li	1.1022	2.22	32.98
Li_4SiO_4	0.9934	0.69	26.65
Li_2TiO_3	0.9758	0.69	27.06

Table 5.3. Summary of optimal results for total TBR and DPA rate in all four blankets. The TBR in the liquid blankets is higher than that in the solid blankets because the liquid blankets also act as their own coolant which provides moderation and breeding in the cooling channel of the double-walled VV. DPA rate is comparable in all four blankets, and is assessed for one FPY.

Considering only the TBR in the liquid blankets, the TBR nearly meets the threshold of 1.1 mentioned in Chapter 3 in both liquid blankets. Recalling that the blanket thickness at the midplane was optimized as explained in the previous chapter, this would not necessarily be the case in an actual reactor such as ARC, which would require a skewed ratio of inboard and outboard blanket thickness to minimize the major radius. However, the vacuum vessel design for the MCNP model is clearly not optimized, especially in the inboard corners that would be far more rounded and would add a significant amount of blanket material in the blanket tank.

The low DPA rate values for the waveguides indicate that as mentioned above, the blanket (regardless of material) does an excellent job of moderating the neutrons in the outboard corner. Based on the irradiation lifetimes quoted in Chapter 2, the waveguides, if placed in the outboard corner, would be lifetime components, assuming a reactor lifetime of around 40 FPY. For the antenna, the DPA values indicate lifetimes around one FPY, based off the 20-25 maximum DPA values mentioned in Chapter 2. For helium concentration, the irradiation lifetime is unclear, but assuming the conservative value of 500 appm, the lifetime would be about four FPY. Of course finding out the lifetime of such components due to degradation from helium accumulation is precisely the reason to have an FNSF. The ARC conceptual design assumed replacement of the vacuum vessel, including the waveguides and antenna, approximately every year [1]. Depending on the engineering design, this may not be required for the waveguides. Since the antenna is placed directly in the vacuum vessel, it would be replaced anyway.

5.3 Comparison of two different waveguide structures

In Section 3.2, two different designs for waveguides were discussed: the main design used for this study (shown in Figure 3.2) in which the waveguide comes in vertically from the top of the blanket tank and a small section reaches the vacuum vessel at an angle, and a traditional design (shown in Figure 3.1) in which the waveguide comes in from near the midplane and bends at right angles into the vacuum vessel directly at the midplane.

The former design was chosen for this study for two reasons. First, in the ARC model, the waveguides are assumed to come into the vacuum vessel through the support post shown in Figure 2.2. The stripped model places them to either the inboard or the outboard side to create a symmetric design so that the inboard and outboard results can be compared correctly. Second, the latter design cannot be applied to the inboard side; there is too little access space which is needed for the toroidal field magnets, central plug, and insulation to have a port at the inboard midplane for waveguides.

In order to compare this study's design and the traditional design, only results for the outboard midplane were compared, using FLibe as the coolant and blanket, eliminating the molybdenum coating. TBR was not considered because the stripped model clearly displaces more blanket, lowering the TBR. The results from both the stripped model and the traditional model are given in Table 5.4 below.

Model	DPA/yr, antenna	DPA/yr, waveguide	He (appm) in antenna	He (appm) in waveguide	DPA/yr, tank	He (appm) in tank
Stripped	47.34	6.75	273.80	4.15	0.027	0.101
Traditional	47.35	9.83	273.82	11.94	0.027	0.101

Table 5.4. Summary of results comparing a traditional waveguide model (coming in from the outboard midplane) and the waveguide design in the stripped model used for this study. DPA and helium concentration are comparable in the antenna, which was not changed in the two designs. The traditional design has a higher DPA rate and more helium retention in the waveguides.

As can be seen from Table 5.4, DPA rate and helium concentration are comparable in the antenna. The design of the antenna did not change between the two designs and since any neutrons coming from the plasma would likely encounter the antenna before reaching the

waveguides or blanket, this result is expected. However, a significant difference is seen in both the waveguides and the blanket tank. In the traditional design, the waveguides are essentially located at the midplane, where neutron flux is highest, and come straight in allowing free-streaming neutrons in part of the waveguides; in the stripped model design, blanket surrounds a large portion of the waveguides and moderates neutrons before they reach the waveguides. The free-streaming neutrons travel through less blanket before reaching the tank, whereas in the stripped model design they do not. This contributes to a higher DPA rate and helium concentration in both the waveguides and the blanket tank when using the traditional design for waveguides.

Chapter 6

Vacuum vessel and waveguide activation

In this chapter, activation of the vacuum vessel and waveguides is discussed. In Section 6.1, how to compute the activity of an isotope as a function of neutron flux and activation cross section is presented. In Section 6.2, the EASY 2010 package and FISPACT code used to perform the activation analysis is discussed, and the inputs used to perform the calculation are described. In the Section 6.3, results for the activity and decay heat as a function of time for one week, one month, and one year of irradiation and compare those results to similar ones obtained for JET and Aries are presented. Finally in Section 6.4, activation results for the antenna and waveguides when the launchers in the outboard midplane are compared to when the launchers are placed in the inboard corner.

6.1 Activation equations and EASY 2010

We first begin with a general expression for the activity of some material where the activity is measured in decays/second. Each isotope in the material will have a different abundance or concentration and decay constant. The number of atoms of a particular isotope can be computed by knowing the mass of the element, m (in grams), the atomic weight of the element, w, and the isotope abundance, a_i:

$$N_i = \frac{m}{w} a_i \mathrm{N_A},$$

where $\mathrm{N_A}$ is Avogado's number. A general expression for the activity in that isotope is just [44]:

$$A_i = \lambda N_i,$$

where λ is the decay constant for the isotope with units of sec^{-1}.

The change in N_i is simply directly proportional to N_i itself, with the constant of proportionality being the decay constant multiplied by the length of time [44]:

$$\Delta N_i = \lambda N_i \Delta t.$$

This is true since each decay is a random, independent event. Given enough events, we can convert this into a differential equation and integrate. The result is the decay equation [44]:

$$N_i = N_{i,0} e^{-\lambda t},$$

where we have incorporated an initial number of isotopes, $N_{i,0}$. The activity as a function of time is simply obtained by multiplying both sides by the decay constant:

$$A_i = A_{i,0} e^{-\lambda t}.$$

Let us now consider what happens when we are actively irradiating some material. The activity equation will now contain two parts, the same general form as above for atoms that are decaying and a second contribution recognizing that there is more activity generated as more neutrons stream into the material. In a reactor situation, the neutron flux is likely known, Φ (in neutrons/cm^2/sec) and the activation cross section of the neutrons and the isotopes in question, σ_i. In this case, the activity is now [45]:

$$A_i = N_i \sigma_i \Phi \left(1 - e^{-\lambda t_{irr}}\right),$$

where t_{irr} is the time during irradiation. Once the irradiation has stopped, the activity becomes:

$$A_i = N_i \sigma_i \Phi \left(1 - e^{-\lambda t_{irr}}\right) e^{-\lambda t_s},$$

where t_s is the time after stopping. Finally, we have considered the activity from one isotope. To obtain the total activity, the activities from every isotope must be summed.

6.2 Input methodology

The EASY 2010 package, and specifically the FISPACT activation code [46, 47], was used to perform the activation analysis for this thesis. The code essentially implements the activation equations above and similar quantities using extensive cross section libraries and follows decay chains through to stable isotopes. The computations require knowledge of the average neutron flux as a function of energy for a specified region, since activation will only occur for neutrons of certain energies, depending on the isotope in question. It also requires knowledge of the material being irradiated and the length of time for irradiation.

For this study, the Vitamin-J energy group structure for the neutron energy spectrum was chosen, as ITER and JET have employed the same structure. There are a total of 175 energy groups, which range from 10^{-7} MeV to 19.6 MeV. They are listed in the FISPACT manual [47]. The energy spectrum is obtained by finding the average neutron flux for the region of interest with MCNP. Since the activation of the vacuum vessel without the presences of waveguides or the antenna is considered first, the energy spectra for the plasma-facing tungsten first wall, the inner Inconel 718 vacuum vessel, and the outer Inconel 718 vacuum vessel, using FLiBe as the coolant and blanket (Figure 6.1), have been obtained. As can be seen from the figure, there is a large peak at 14.1 MeV since most fusion neutrons will pass right through the vessel components into the blanket. However, moving radially outward, we see a reduction in the total flux and in the flux at the 14.1 MeV peak, meaning that some neutrons are absorbed by the materials in each region. The relatively large reduction in fluence into the outer vacuum vessel shows that a significant fraction of the neutrons are absorbed in the cooling channel and beryllium layers. These values are given in Table 6.1.

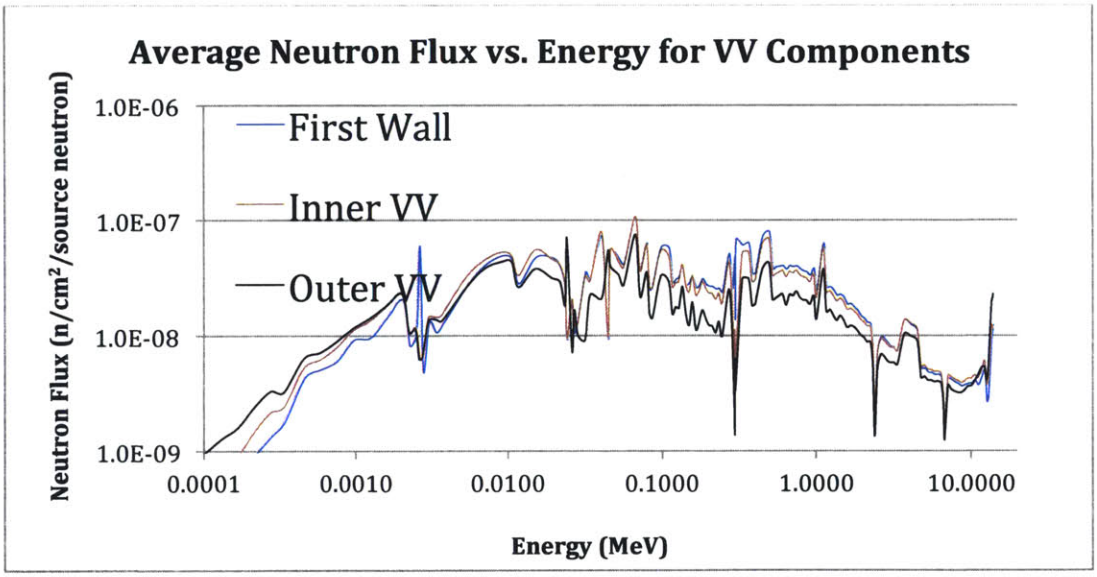

Figure 6.1. Average neutron fluence ($1/cm^2/MeV$) vs. energy (MeV) for the tungsten first wall (blue), inner vv (red), and outer vv (black).

Region	Total neutron fluence (n/cm^2/source neutron)	Peak neutron fluence at 14.1 MeV (n/cm^2/source neutron)
First wall	3.94×10^{-6}	5.48×10^{-7}
Inner vacuum vessel	3.50×10^{-6}	4.20×10^{-7}
Outer vacuum vessel	2.38×10^{-6}	1.60×10^{-7}

Table 6.1. Total and peak neutron fluxes for the first wall and inner and outer vacuum vessels, computed with MCNP. The VITAMIN-J energy group structure was used.

To evaluate the activation in the vacuum vessel, the fluences obtained with MCNP were input into FISPACT as a flux file, after multiplying by the number of neutrons produced every second in an ARC-like reactor assuming 525 MW of fusion power. Each region was treated separately. Three different irradiation times were chosen: one week, one month (30 days), and one year. This gives a total of nine FISPACT runs. After irradiation, the flux is set to zero, and the activation and heating are measured at regular intervals of one day, 30 days, six months, one year, two years, five years, and ten years after irradiation. An example of a FISPACT input file is given in Appendix 3.

Second, differences in activation of the blanket and the waveguides and antenna between the optimal poloidal launcher location we found in Chapter 5 in the inboard corner and the launcher location at the outboard midplane are considered, using the stripped model design for the waveguides. The same process was used to obtain the fluences in the FLiBe cooling channel, FLiBe blanket, waveguides, and antenna for both launcher locations. The total neutron fluences and neutron fluences at 14.1 MeV are given in Table 6.2 below.

Region	Total neutron fluence (n/cm^2/source neutron)	Neutron fluence at 14.1 MeV (n/cm^2/source neutron)
FLiBe cooling	3.095×10^{-6} 3.093×10^{-6}	3.10×10^{-7} 3.14×10^{-7}
FLiBe blanket	1.89×10^{-7} 1.88×10^{-7}	8.25×10^{-9} 8.30×10^{-9}
Antenna	4.55×10^{-6} 3.30×10^{-6}	6.03×10^{-7} 2.71×10^{-7}
Waveguides	8.57×10^{-7} 3.85×10^{-7}	3.22×10^{-8} 6.00×10^{-9}

Table 6.2. Total neutron fluence and neutron fluence at 14.1 MeV. Values for the outboard midplane launcher location are given first and values for the inboard corner launcher location are given second.

Looking at Table 6.2, fluences in both the waveguides and the antenna are much smaller when the launcher is placed in the inboard corner rather than the outboard midplane. This is consistent with our results in Chapter 5. In the cooling channel and blanket, the fluences at 14.1 MeV are larger rather than smaller when the launchers are placed at the outboard midplane. This is because more moderation occurs on the outboard side; the antenna is placed at the midplane where most neutrons are directed leaving the plasma and the outboard blanket is thicker than the inboard blanket.

6.3 Vacuum vessel activation results

For each of the nine FISPACT runs, FISPACT output includes the total activity and the total decay heat as a function of time. Peak values as well as values after 10 years for all three regions and one week, 30 days, and one year of irradiation are given in Table 6.3 for the activity, decay heat, and the total inhalation and ingestion dose. For each scenario, the peaks are measured immediately after irradiation.

In general, all three quantities decrease by several orders of magnitude over the ten-year period, decaying the most within the first year, indicating the dominance of isotopes with ~100 day half-lives. For all three regions, the peak activity increases with irradiation time; the same holds true for the first wall after ten years, but in the inner and outer vacuum vessels, the ten-year activity after seven days of irradiation is greater than it is after 30 days of irradiation. In all three regions, the peak decay heat increases with irradiation time. And regarding the dose rate, in all cases, to reach mSv level requires at least a few years after irradiation.

Comparing between the inner and outer vacuum vessels for the three irradiation times, in general, all three quantities are lower in the outer vacuum vessel where more neutrons have been moderated in the cooling and beryllium layers. All three regions are below the IAEA recycling limit of 10^{-2} Sv/hr [48] essentially immediately after irradiation. However, the total activity of Inconel 718 is in general an order of magnitude worse compared to other proposed structural materials such as low-activation steels, vanadium, and silicon-carbide [49].

Scenario	Peak activity (Bq/kg)	Activity at 10 years (Bq/kg)	Peak decay heat (W/kg)	Decay heat at 10 years (W/kg)	Peak dose* (Sv)	Dose* at 10 years (Sv)
First wall, 7 days	$3.18\text{x}10^{14}$	$9.12\text{x}10^{7}$	21.6	$6.00\text{x}10^{-7}$	$4.80\text{x}10^{9}$	$4.75\text{x}10^{3}$
First wall, 30 days	$4.01\text{x}10^{14}$	$3.87\text{x}10^{8}$	23.1	$2.55\text{x}10^{-6}$	$6.46\text{x}10^{9}$	$2.03\text{x}10^{4}$
First wall, 1 year	$7.77\text{x}10^{14}$	$3.83\text{x}10^{9}$	30.0	$2.60\text{x}10^{-5}$	$1.45\text{x}10^{10}$	$2.20\text{x}10^{5}$
Inner VV, 7 days	$1.67\text{x}10^{14}$	$5.72\text{x}10^{10}$	24.2	$6.03\text{x}10^{-3}$	$1.50\text{x}10^{9}$	$1.04\text{x}10^{7}$
Inner VV, 30 days	$2.68\text{x}10^{14}$	$2.45\text{x}10^{11}$	31.2	$2.58\text{x}10^{-2}$	$3.94\text{x}10^{9}$	$4.42\text{x}10^{7}$
Inner VV, 1 year	$5.46\text{x}10^{14}$	$2.70\text{x}10^{12}$	56.7	$2.94\text{x}10^{-1}$	$1.56\text{x}10^{9}$	$5.04\text{x}10^{8}$
Outer VV, 7 days	$1.17\text{x}10^{14}$	$2.91\text{x}10^{10}$	12.5	$3.27\text{x}10^{-3}$	$2.53\text{x}10^{9}$	$1.73\text{x}10^{7}$
Outer VV, 30 days	$1.54\text{x}10^{14}$	$1.25\text{x}10^{11}$	16.4	$1.40\text{x}10^{-2}$	$6.82\text{x}10^{9}$	$7.41\text{x}10^{7}$
Outer VV, 1 year	$2.99\text{x}10^{14}$	$1.39\text{x}10^{12}$	30.9	$1.60\text{x}10^{-1}$	$2.66\text{x}10^{10}$	$8.46\text{x}10^{8}$

Table 6.3. Activity, decay heat, and *total inhalation and ingestion dose immediately after irradiation and ten years after irradiation, for all nine scenarios. These were computed with no waveguides present.

In Tables 6.4 and 6.5, the dominant nuclides immediately after irradiation and after 10 years, respectively, are provided along with their percentage contribution to the total activity and their half-lives. The dominant nuclides are similar between the inner and outer vacuum vessel for the three irradiation times, respectively, as is to be expected since the inner and outer vessels are both composed of Inconel 718. Dominant nuclides in all three regions tend to differ the most between an irradiation time of seven days and of 30 days. There is little difference between dominant nuclides after 30 days of irradiation versus after a year of irradiation. Comparing between the two tables, immediately after irradiation, the dominant nuclides have much shorter half-lives than compared to those existing after ten years. This is to be expected since nuclides with short half-lives will burn off quickly, leaving only nuclides with longer half-lives after some length of time. It is also important to notes that only just a few nuclides in most cases produce most of the activity, more than 50% for three or four nuclides.

Scenario	Dominant nuclides	Percentage of total activity	Half-life
First wall, 7 days	W-187	36.2	1 day
	W-183m	31.3	5.3 sec
	W-185m	23.2	1.7 min
First wall, 30 days	W-187	28.9	1 day
	W-183m	24.9	5.3 sec
	W-185m	19.8	1.7 min
First wall, 1 year	W-185	40.2	75.1 days
	W-181	21.6	121 days
	W-187	14.7	1 day
Inner VV, 7 days	Co-58m	41.5	8.9 hrs
	Nb-94m	10.2	2.3 min
	Mn-56	9.5	2.6 hrs
	V-52	7.2	3.7 min
Inner VV, 30 days	Co-58m	30.2	8.9 hrs
	Co-58	17.2	70.9 days
	Cr-51	8.9	27.7 days
Inner VV, 1 year	Co-58	32.3	70.9 days
	Co-57	20.5	272 days
	Co-58m	15.1	8.9 hrs
Outer VV, 7 days	Co-58m	31.6	8.9 hrs
	Co-58	17.7	70.9 days
	Nb-94m	11.7	2.3 min
	Cr-51	6.9	27.7 days
Outer VV, 30 days	Sr-87m	20.7	2.8 hrs
	Ba-137m	13.5	2.6 min
	Ba-136m	13.4	0.31 sec
Outer VV, 1 year	Sr-87m	19.6	2.8 hrs
	Ba-137m	13.1	2.6 min
	Ba-136m	12.9	0.31 sec
	Xe-135m	1.0	15.3 min

Table 6.4. Dominant nuclides, percentage of total activity, and half-lives for all nine scenarios, *immediately after irradiation*. The dominant nuclides are similar between the inner and outer vacuum vessel for the three irradiation times, respectively, as is to be expected since the inner and outer vessels are both composed of Inconel 718.

Scenario	Dominant nuclides	Percentage of total activity	Half-life
First wall, 7 days	Ta-179	98.1	1.6 years
	Tritium	1.5	12.3 years
First wall, 30 days	Ta-179	98.1	1.6 years
	Tritium	1.5	12.3 years

First wall, 1 year	Tl-179	97.6	1.6 years
	Tritium	1.8	12.3 years
Inner VV, 7 days	Fe-55	65.8	2.7 years
	Co-60	25.0	5.3 years
	Nb-93m	6.8	16.1 years
Inner VV, 30 days	Fe-55	65.8	2.7 years
	Co-60	25.0	5.3 years
	Nb-93m	6.8	16.1 years
Inner VV, 1 years	Fe-55	64.5	2.7 years
	Co-60	25.8	5.3 years
	Nb-93m	7.3	16.1 years
Outer VV, 7 days	Fe-55	61.6	2.7 years
	Co-60	26.7	5.3 years
	Nb-93m	8.9	16.1 years
Outer VV, 30 days	Fe-55	61.6	2.7 years
	Co-60	26.7	5.3 years
	Nb-93m	9.0	16.1 years
Outer VV, 1 year	Tritium	88.6	12.3 years
	Kr-85	0.76	10.8 years
	Co-60	0.10	5.3 years

Table 6.5. Dominant nuclides, percentage of total activity, and half-lives for all nine scenarios, *ten years after irradiation.* The dominant nuclides are similar between the inner and outer vacuum vessel for the three irradiation times, respectively, as is to be expected since the inner and outer vessels are both composed of Inconel 718.

6.4 Waveguide and antenna activation results

Again, the second test involves comparing activation when the launchers are placed at the outboard midplane versus when they are placed at the inboard corner, the optimal location we found in Chapter 5.

Similar FISPACT analysis was performed, with one year of irradiation (the planned amount of time before replacement of the vacuum vessel), using the MCNP-computed fluxes in the cooling channel, blanket, waveguides and antenna. Results for the activity, decay heat, and total inhalation and ingestion dose rate are given in Table 6.6.

Scenario	Peak activity (Bq/kg)	Activity at 10 years (Bq/kg)	Peak decay heat (W/kg)	Decay heat at 10 years (W/kg)	Peak dose* (Sv)	Dose* at 10 years (Sv)
Blanket, outboard	$3.54\text{x}10^{13}$	$9.64\text{x}10^{12}$	14.1	$8.82\text{x}10^{-3}$	$4.38\text{x}10^{9}$	$2.33\text{x}10^{9}$
Blanket, inboard	$3.56\text{x}10^{13}$	$9.57\text{x}10^{12}$	14.3	$8.75\text{x}10^{-3}$	$4.35\text{x}10^{9}$	$2.33\text{x}10^{9}$
Cooling, outboard	$6.07\text{x}10^{14}$	$1.85\text{x}10^{14}$	197	0.17	$8.52\text{x}10^{8}$	$4.51\text{x}10^{8}$
Cooling, inboard	$6.10\text{x}10^{14}$	$1.85\text{x}10^{14}$	199	0.17	$8.51\text{x}10^{8}$	$4.50\text{x}10^{8}$
Waveguide, outboard	$9.38\text{x}10^{13}$	$3.94\text{x}10^{11}$	9.9	0.04	$2.58\text{x}10^{9}$	$6.99\text{x}10^{7}$
Waveguide, inboard	$2.45\text{x}10^{13}$	$9.81\text{x}10^{10}$	2.4	0.01	$1.22\text{x}10^{8}$	$3.40\text{x}10^{6}$
Antenna, outboard	$7.95\text{x}10^{14}$	$3.81\text{x}10^{12}$	77.9	0.41	$2.21\text{x}10^{9}$	$7.24\text{x}10^{7}$
Antenna, inboard	$3.77\text{x}10^{14}$	$1.86\text{x}10^{12}$	38.1	0.20	$1.10\text{x}10^{9}$	$3.64\text{x}10^{7}$

Table 6.6. Activity, *total inhalation and ingestion dose, and decay heat immediately after irradiation and ten years after irradiation for the blanket, cooling channel, waveguides, and antenna. Outboard refers to placing the launchers in the outboard midplane location while inboard refers to placing them in the inboard corner. There is a significant reduction in all three quantities when the launchers are placed in the inboard corner.

Looking at Table 6.6, there were essentially no differences in activation, decay heat, and dose rate in the cooling channel and blanket between the two launcher locations. However, there is a significant reduction in all three quantities when the launchers are placed in the inboard corner versus the outboard midplane. In the antenna, all three quantities are reduced by a factor of two. In the waveguides, the reduction is even larger, by a factor of four. This is consistent with the results obtained in Chapter 5, since the DPA and the helium production were reduced by a factor of two.

Dominant nuclides were similar in the waveguides and antenna to those in the vacuum vessel since the waveguides/antenna are also composed of Inconel 718. Dominant nuclides in the cooling channel and blanket for the outboard scenario are reported in Table 6.7.

Scenario	Dominant nuclides	Percentage of total activity	Half-life
Blanket, after irradiation	Tritium	47.7	12.3 years
	N-16	26.2	7.1 sec
	He-6	8.4	0.81 sec
Blanket, 10 years after irradiation	Tritium	100	12.3 years
Cooling channel, after irradiation	Tritium	53.4	12.3 years
	N-16	20.1	7.1 sec
	F-18	10.4	1.8 hrs
Cooling channel, ten years after	Tritium	100	12.3 years

Table 6.7. Dominant nuclides, percentage of total activity, and half-lives for the blanket and cooling channel whn the launchers are placed at the outboard midplane.

The results in Table 6.7 are completely expected. The FLiBe blanket and cooling channel need to breed tritium, and given that it is the dominant nuclide both immediately after irradiation and after ten years proves the blanket serves its purpose. Of course, the tritium should not be included as contributing to actual activation since it is removed from the blanket in a recovery process and reused as fuel for the reactor.

Chapter 7

Summary, future work, and conclusions

A summary of the original research question and results is given in Section 7.1. Caveats regarding the MCNP and activation models and results as well as suggestions for future work are given in Section 7.2. Final conclusions are provided in Section 7.3.

7.1 Summary of the original research question and results

This thesis began by introducing an issue which has arisen recently as work has begun to propose the next generation of tokamak fusion devices to come after ITER, namely heating the plasma and driving current. The best methods for accomplishing those tasks involve launching waves at various frequencies directly into the plasma. Launching these waves requires a wave source, waveguides to carry the waves through the reactor, and an antenna or launcher to release the wave into the plasma. Typically these launchers must be placed inside the vacuum vessel as close to the plasma as possible, leaving them (and the waveguides) particularly susceptible to radiation damage from the highly energetic neutron products of the fusion reactions powering the reactor. Past research has indicated that there exists an optimal placement of the waveguides and antennas to maximize current drive efficiency, allow for better wave penetration, and have favorable plasma turbulence characteristics [4], namely the inboard or high-field side of the tokamak near an active X-point rather than the traditional outboard, low-field midplane. Several recent reactor designs have proposed launching waves from the inboard side, including ARC, ADX, and Vulcan [1-3]. *The question remains, does placing the waveguides and launchers on*

the inboard side also reduce their radiation damage and help to maximize the tritium breeding necessary to generate the fuel to power the reactor?

To answer this question, the number of neutrons the launchers and waveguides see every second needs to be computed and how they interact with the material atoms in the launchers and waveguides needs to be examined. This lends itself to using MCNP, the Monte Carlo Neutral Particle transport code [11], to solve for the neutron fluences and fluxes, which can then be used to tally certain reactions: tritium breeding in a reactor blanket, and damage reactions in the form of displacements per atom and helium production/retention through transmutation. The equations used to compute these reactions and tallies were covered in Chapter 3. MCNP requires inputting a model of some reactor geometry and will compute tallies for that model. This study was inspired by the ARC reactor design and ARC's MCNP model was used as the starting point. The basics of ARC as it pertains to this thesis were covered in Chapter 2 and its radial build was presented, using the MCNP model as a visual representation. To place the MCNP results in context with what are acceptable levels of damage and the minimum amount of tritium breeding to sustain reactor operation, recent damage and TBR results from the literature was also discussed in Chapter 2. Our own stripped MCNP model was presented in Chapter 3, explaining the new D-shaped vacuum vessel and the waveguide and antenna design.

To answer the question as rigorously as possible, seven locations around the vacuum vessel were chosen, starting with the outboard midplane and working around to the inboard midplane, noting that the outboard midplane is where traditional reactor designs place the waveguides and launchers. A map of these locations is shown in Figure 3.4. Four different blanket materials were also chosen, two solid blankets and two liquid blankets, to test whether or not the material phase would affect the optimal location. A table of the four blanket materials with compositions and properties is given in Table 3.3.

The first MCNP results were not necessarily to answer the original question, but to explore the general neutronics of a fusion blanket, specifically to understand how tritium breeding is impacted by blanket thickness as measured by the distance from the plasma and as measured by its absolute thickness on either the inboard or the outboard side. The importance of including a neutron multiplier was also explored. Not only did these results help refine the MCNP model, but they can serve as a guide for future blanket designs and help the reader gain

an intuition for how changes in the blanket design will affect quantities of interest. We summarize those results now.

1) The thinner the structural material between the plasma and the blanket, the higher the TBR. Most breeding takes place within the first 70 cm of blanket material and most of the increase in TBR as a function of distance from the plasma takes place within the first 40 cm for efficient moderators with only low-Z elements.
2) Inclusion of a neutron multiplier boosts TBR substantially. For example, in our stripped model with FLiBe, removing the beryllium multiplier layer of the vacuum vessel and replacing with FLibe decreased the TBR by 10%. Adding an extra centimeter of beryllium multiplier increased TBR by 6%. These are significant increases to TBR.
3) In a reactor with a finite-sized blanket tank, at the midplane, the optimal blanket thicknesses (distance from tank to edge of the vacuum vessel) are to have a slighter thicker blanket on the outboard side than on the inboard side. For example, in our model, the TBR was maximized when the inboard thickness was 45 cm and the outboard thickness was 55 cm. A thinner inboard blanket (and thicker outboard blanket) reduced the TBR. We note that this changes the major radius of the vacuum vessel.

Having established these ground rules, we are finally in a position to determine the optimal location of the waveguides and the antenna. Having completed 28 different MCNP runs, four blankets and seven locations, we summarize the results below:

1) The optimal location of the antenna/launcher is in the inboard corner, as measured by minimal DPA and helium retention.
2) The optimal location of the waveguides depends on the quantity considered. To minimize DPA, the waveguides must be placed in the outboard corner. To minimize helium retention, they must be placed in the inboard corner.
3) Given that the antenna is best placed in the inboard corner, the waveguides should obviously be placed there.

4) TBR is maximized when the waveguides and antenna are placed at the top of the vacuum vessel, or in the inboard corner. However, only a small amount of TBR is lost if the waveguides and antenna are placed elsewhere around the vacuum vessel.
5) When placed in the inboard corner as opposed to the tradition outboard midplane, the damage is generally reduced by a factor of two, indicating a significant to the expected lifetime of these components.
6) The waveguide design itself makes a difference in the damage rate. For an antenna at the outboard midplane, having the waveguides enter from the top of the vacuum vessel as opposed to entering from the outboard midplane also significantly reduces the damage, even though more material is used in the former design.
7) The optimal location does not depend on blanket phase or material. Results were essentially the same for all four blankets, so the previous six points can be applied universally.
8) Placing the launchers in the inboard corner reduces activation by a factor of two in the antenna and a factor of four in the waveguides, when compared to placing them near the outboard midplane.

Regarding the original question (*does placing the waveguides and launchers on the inboard side also reduce their radiation damage and help to maximize the tritium breeding necessary to generate the fuel to power the reactor?*), the answer is yes. Placing the waveguides and launcher on the inboard side, especially in the upper corner, reduces damage and activation and maximizes TBR. Given the small absolute affect on TBR, the main factor in the decision is damage reduction. That said, we can now say that placing the RF antennas/launchers in the inboard corner improves performance in several areas: 1) better wave penetration and current drive efficiency, 2) better plasma turbulence and plasma-materials interaction characteristics, 3) reduced radiation damage due to atomic displacements and transmutations, and 4) reduced activation.

7.2 Caveats and future work

While this study has successfully demonstrated that the inboard upper corner of a vacuum vessel is the optimal location for waveguide and launchers to minimize radiation damage and maximize tritium breeding, this study does have limitations. We list and discuss them below.

1) The MCNP model used is a two-dimensional model. In other words, the surfaces and cells used to mimic the components of the vacuum vessel and blanket tank were only defined in the Z- and R- dimensions and were assumed to be toroidally continuous. This includes the waveguides and launchers. In a real reactor, the waveguides and launchers would not be toroidally continuous; they will have a finite length as well as width and thickness. A 3-D MCNP model will need to be constructed to verify that the 2-D results carry over.
2) The waveguide and launcher have been oversimplified. In the stripped model, we modeled the waveguide structural material and empty space as simply structural material at half the density. While this provides an estimate of the damage, it assumes that the damage will be spread across the entire region, when in reality the damage is only in the surrounding structural material. This also affects the damage to the blanket tank, since any free-streaming neutrons will pass right through to the tank. The tank will experience more localized damage.
3) The waveguides' locations of entry at the top of the blanket tank may not be realistic or optimized. Currently, the waveguides enter the top of the tank from either the inboard or the outboard side, not close to the vacuum vessel. A more realistic design would have the waveguides coming in closer to the vessel, or in the case of ARC, the waveguides will come in from a support post at the top and along the sides. The exact location of the waveguides, however, will not affect the optimal location of the antenna.
4) The D-shaped vacuum vessel is not optimized. For example, the corners of the D are too sharp; a realistic D-shape will have softened corners. This may slightly affect the optimal location of the waveguides and antenna in the inboard corner.

5) The stripped model does not include an upper divertor. We assumed a single-null plasma equilibrium for our source input, which only necessitated using a divertor at the bottom of the vacuum vessel. Other designs and perhaps a real reactor will allow for a double-null plasma equilibrium. The true divertor shape may affect the neutron flux entering the vacuum vessel, which may modify the optimal location of the waveguides and launchers.
6) Our stripped model is based off of the original MCNP ARC model, which included a double-walled vacuum vessel designed to have a liquid FLiBe cooling channel and a blanket tank surrounding the liquid blanket. Recalling from Chapter 2 that solid blankets only need a plasma-facing first wall and a vacuum vessel surrounding the blanket, our stripped model is not representative of a true solid blanket design which may affect the results for the two solid blankets.

For future work, all six points must be addressed, along with further refining the optimal location in the inboard corner. To do this, the 2-D model must be converted into a 3-D model, finding a realistic length for the waveguides and launcher and adjusting the width as needed. The waveguide and launcher designs as well as the D-shape will likely need to be created as a CAD model and imported into MCNP, which will generate new surfaces and cells to represent the new shapes and regions. Further refinement of the optimal location will involve performing a similar set of tests as completed in this thesis, but choosing angles between 100° and 140°. The sixth point can only be tested once a FNSF is built.

One other future test, which does not have an associated caveat, is related to the optimal placement of the vacuum vessel within the blanket tank. In using a distance of 45 cm between the blanket tank and the inboard midplane of the vacuum vessel, the major radius of the ARC reactor changed. However, that distance originally was only 20 cm. Adding 25 cm of blanket has a tremendous impact on the damage to the blanket tank, insulating layer, and magnets. In fact, the neutron shield may not need to be as thick as it is after adding the 25 cm of blanket. Reducing the thickness of the neutron shield, which is currently 50 cm, may bring the major radius closer to the original. In other words, it may be possible to achieve the same shielding by trading the neutron shield for more blanket. This should be tested in MCNP.

7.3 Conclusions

To conclude the thesis, our results can be placed in a greater context with respect to reactor design. Inboard corner launch is not only good for current drive efficiency and wave penetration which greatly affect the plasma physics aspects of the design, but it is also good for damage, activation, and fuel breeding, the nuclear and energy generation aspects of the design. Traditional designs have always placed the waveguides/launchers at the outboard midplane, but this is incorrect, and will actually increase the damage by a factor of two compared to placing them at the inboard corner, requiring replacement more often and having an adverse effect on how the waves are absorbed by the plasma. Vulcan, ADX, and ARC are the first major designs to implement high-field side launch and this thesis validates that choice. We hope to see future designs from other groups implement high-field-side launch. These results underscore the need to perform experiments on existing machines with high-field-side waveguides and launchers to demonstrate that all mentioned benefits are experimentally feasible.

Along with these results are those regarding blanket thicknesses. It has been demonstrated that a blanket only needs to be about 70 cm thick to maximize TBR, and the placement of the vacuum vessel within the blanket tank should actually favor only a slightly larger thickness on the outboard side, keeping in mind that adjusting the placement affects the major radius. Since high TBR is difficult to achieve regardless of blanket material used, these small adjustments can make a difference in breeding enough tritium for operation. Since only 70 cm is required for maximum TBR in most blankets, this says that anything beyond 70 cm just adds to the cost of extra materials for a larger blanket tank and blanket.

These particular points about the waveguide/launcher location, blanket thickness, and activation help to constrain a future fusion reactor design. With upcoming experiments such as ITER, and proposed experiments such as ADX, further constraints will be placed. There should have a clearer picture of what the first fusion power plant will look like in the next decade or so.

Bibliography

[1] B. N. Sorbom et al. ARC: A compact, high-field fusion nuclear science facility and demonstration power plant with demountable magnets. *Fusion Engineering and Design*, 100: 378-405, 2015.

[2] B. LaBombard, et al. ADX: A high field, high power density, advanced divertor and RF tokamak. *Nuclear Fusion*. 55: 053020, 2015.

[3] Y. Podpaly et al. The lower hybrid current drive system for steady-state operation of the Vulcan tokamak conceptual design. Fusion Engineering and Design, 87: 215-223, 2012.

[4] G. Wallace. High field side launch of RF waves: A new approach to reactor actuators, *In 21st Topical Conference on Radiofrequency Power in Plasmas*, Lake Arrowhead, CA, 2015.

[5] J. Freidberg. *Plasma Physics and Fusion Energy*, pages 16-19. Cambridge University Press, Cambridge, UK, 2007.

[6] D. A. Gurnett and A. Bhattacharjee. *Introduction to Plasma Physics*, pages 2–3. Cambridge University Press, Cambridge, UK, 2005.

[7] CEA, 2006. Retrieved November 30, 2015 from WWW. URL: http://www-fusion-magnetique.cea.fr/gb/fusion/physique/configtokamak.htm

[8] J. M. Sierchio. *Comparison of Edge Turbulence Velocity Analysis Techniques Using Gas Puff Imaging Data on Alcator C-Mod.* SM thesis. Massachusetts Institute of Technology, 2014.

[9] R. E. Krebs, *The History and Use of Our Earth's Chemical Elements: A Reference Guide*. Greenwood Press, Westport, CT, 2006.

[10] EFDA PPCS, 2005. Retrieved on December 1, 2015 from WWW. URL: http://bpe.epfl.ch/page-34027-en.html

[11] T. H. Stix. *Waves in Plasmas*. Springer-Verlag, New York, NY, 1992.

[12] F. B. Brown et al. MCNP version 5, Transactions of the American Nuclear Society 87: 4, 2002.

[13] Y. Poitevin. The Tritium Breeding Blankets for Fusion Reactors: A key component for sustainability of Fusion Energy. In *Fusion for Energy*, Barcelona, Spain, March 2011. Swiss Nuclear Forum.

[14] F. Najmabadi et al. The ARIES-AT advanced tokamak, Advanced technology fusion power plant. *Fusion Engineering and Design,* 3: 23, 2006.

[15] G. R. Odette and D. T. Hoelzer. Development of Nanocomposed Ferritic Alloys for High Performance Fusion First Wall and Blanket Structures. *In American Nuclear Society Fusion Energy Division Newsletter*, June 2002. Retrieved December 4, 2015 from WWW. URL: http://fti.neep.wisc.edu/fednews/news0602.pdf

[16] A. R. Raffray et al. Design and materials issues for high-performance SiC_f/SiC-based fusion power cores. *Fusion Engineering and Design*, 55: 55-95, 2001.

[17] S. Reyes, et al. "LIFE Tritium Processing: A Sustainable Solution For Closing the Fusion Fuel Cycle," Lawrence Livermore National Laboratory report, LLNL-TR-576952, 2012. Retrieved December 5, 2015 from WWW. URL: https://e-reports-ext.llnl.gov/pdf/651552.pdf

[18] R.-D. Penzhorn and M. Gugla. Process to Recover Tritium from Fuel Cycle Impurities. *Fusion Science and Technology,* 10:1345, 1986.

[19] V. McLane, C. L. Dunford, and P.F. Rose, ed., "ENDF-102: Data Formats and Procedures for the Evaluated Nuclear Data File ENDF-6," Brookhaven National Laboratory report, BNL-NCS-44945, revised 1995.

[20] L. A. El-Guebaly and the ARIES team. Nuclear performance assessment of ARIES-AT. *Fusion Engineering and Design*, 80: 99-110, 2006.

[21] R. D. Stambaugh. Major Remaining Challenges and Solution Paths. In Fusion Energy Assessment, The Electric Power Research Institute, Palo Alto, CA, 2011. Retrieved December 6, 2015 from WWW. URL: http://fire.pppl.gov/EPRI_MFE_Challenges_Stambaugh.pdf

[22] V. S. Chan et al. Evaluation of CFETR as a Fusion Nuclear Science Facility using multiple system codes. *Nuclear Fusion*, 55: 023017, 2015.

[23] P. Jung, C Liu, and J. Chen. Retention of implanted hydrogen and helium in martensitic stainless steels and their effects on mechanical properties. *Journal of Nuclear Materials* 296: 165, 2001.

[24] A. Moeslang and D. Preininger. Effect of helium implantation on the mechanical properties and the microstructure of the martensitic 12% Cr-steel 1.4914. *Journal of Nuclear Materials*, 155: 1064, 1988.

[25] F. A. Garner et al. Void Swelling at Low Displacement Rates in Annealed X18H10T Stainless Steel at 30-56 DPA and 280-332°C, In *Proceedsings of the Ninth International*

Symposium on Environmental Degradation of Materials in Nuclear Power Systems - Water Reactors, Newport Beach, CA, 1999.

[26] M. Vuolo et al. Evaluation of the Neutron Activation of Jet In-vessel Components Following DT Irradiation. EFDA–JET–CP(13)05/09, *In Proceedings of the 11th International Symposium on Fusion Nuclear Technology*, Barcelona, Spain, September 2013. EFDA. Retrieved December 20, 2015 from WWW. URL: http://www.euro-fusionscipub.org/wp-content/uploads/2014/11/EFDC130509.pdf

[27] U.S. Nuclear Regulatory Commission. (2015, December 2), 61.55 Waste Classification, Retrieved December 20, 2015 from WWW. URL: http://www.nrc.gov/reading-rm/doc-collections/cfr/part061/part061-0055.html

[28] D. A. Petti et al. Safety and environment assessment of ARIES-AT. *Fusion Technology* 39:449-457, 2001.

[29] The X-5 Monte Carlo Team. *MCNP: A General Monte Carlo N-Particle Transport Code, Version 5*. Los Alamos National Laboratory report LA-UR-03-1987, April 2003.

[30] A. Hogenbirk. An easy way to perform a radiation damage calculation in a complicated geometry. *Fusion Engineering and Design*, 83: 1828-1831, 2008.

[31] G. Wallace and S. Wukitch, personal communication, June 2015.

[32] S. J. Zinkle. Summary of Physical Properties for Lithium, Pb-17Li, and $(LiF)_n \cdot BeF_2$ Coolants. In Apex Study Meeting, Sandia National Laboratory, 1998. Retrieved June 20, 2015 from WWW. URL: http://www.fusion.ucla.edu/ITER-TBM/Documents/liq_coolant_properties_rev.pdf

[33] U. Jauch, G. Haase, and B. Schulz. Thermophysical properties of the Li(17)Pb(83) eutectic alloy, *Kernforschungszentrum Karlsruhe*, 1986.

[34] M. Song et al. Impact of neutronics considerations on the selection of solid breeder and multiplier materials and configurations. Fusion Engineering and Design, 10: 47-55, 1989.

[35] G. R. Hopkins and G. Melese-d'Hospital, Helium Cooling of Fusion Reactors. *Nuclear Engineering and Design,* 26: 215-230, 1974

[36] C. B. Baxi and C. P. C. Wong. Review of Helium Cooling for Fusion Reactor Applications. General Atomics report, GA-A23181, 1999. Retrieved June 30, 2015. URL: https://fusion.gat.com/pubs-ext/MISCONF99/A23181.pdf

[37] W. M. Stacey. Fusion: An Introduction to the Physics and Technology of Magnetic Confinement Fusion, Wiley-VCH, Weinheim, Germany, 2010.

[38] Y. Nomoto et al. Structural concept of Japanese solid breeder test blanket modules for ITER. *Fusion Engineering and Design*, 81: 719, 2006.

[39] D. Meade, A comparison of unit costs for FIRE and ITER, July 2002. Retrieved December 10, 2015 from WWW. URL http://fire.pppl.gov/snow_ITERFIRE_cost.pdf

[40] R. Beck. Research and development of metal hydrides, USAEC report LAR1960-10.

[41] Z. Hartwig. Proposal for Vulcan Star Research, January 2012. PSFC.

[42] H. H. Hausner. "Nuclear Properties," *Beryllium: Its Metallurgy and Properties*. University of California Press, Berkely, CA, 1965.

[43] Simakov, S. (2015, December 29). Primary Radiation Damage Cross Sections. Retrieved January 17, 2016 from WWW. URL: https://www-nds.iaea.org/CRPdpa/

[44] K. S. Krane. *Introductory Nuclear Physics*. John Wiley and Sons, United States, 1988.

[45] P. Ila, Neutron activation analysis fundamental concepts. From Trace Element Analysis of Geological, Biological, and Environmental Materials by Neutron Activation Analysis course notes, January 2005. Retrieved December 20, 2015 from WWW. URL: http://ocw.mit.edu/courses/earth-atmospheric-and-planetary-sciences/12-091-trace-element-analysis-of-geological-biological-environmental-materials-by-neutron-activation-analysis-an-exposure-january-iap-2005/lecture-notes/session1b.pdf

[46] J.-Ch. Sublet, L.W. Packer, J. Kopecky, R.A. Forrest, A. J. Koning, D.A. Rochman, The European activation file: EAF-2010 neutron-induced cross section library, EASY Documentation Series, CCFE-R(10)05, Culham, 2010.

[47] J.-Ch. Sublet, J.W. Eastwood, J.G. Morgan, The FISPACT user manual, CCFE-R(11) Issue 3, Culham Science Centre, 2012.

[48] IAEA "Clearance levels for radionuclides in solid materials: application of exemption principles", interim report for comment, IAEA TECDOC-855, Vienna, January 1996.

[49] D. A. Petti et al. "Re-evaluation of the low activation materials in waste management strategies for fusion," In the *International Symposium on Fusion Nuclear Technology*, Rome, Italy, 1999.

Appendix A

Example MCNP Input

In this appendix, we will provide a sample of the surface and cell cards in the stripped model used to perform the MCNP runs. The example below produces a waveguide and antenna located at the outboard midplane, shown in Figure 3.2 of the thesis. We also include the material card for Inconel 718 (number 9300 in the cell cards). Other material cards are relatively simple to construct.

```
c ********************************************************************
c                    Cell Cards
c
 1    1000 2.4E-10    -9 IMP:N,P=1
 2    1000 2.4E-10    -7 9 IMP:N,P=1
 3    1000 2.4E-10    -5 7 IMP:N,P=1
 4    7000 -19.3      2 -3 -1 IMP:N,P=1
 5    1000 2.4E-10    -1 2 #(2 -3 -1 )#(-5 )#(50 -49 45 2 -1 ) IMP:N,P=1
 6    7000 -19.3      -13 12 #(-1 2 ) IMP:N,P=1  $ First Wall
 7    9300 -8.19      -15 14 #(-13 12 ) IMP:N,P=1  $ VV1
 8    5014 -1.973     -17 16 #(-15 14 ) IMP:N,P=1  $ He cooling
 9    4000 -1.85      -19 18 #(-17 16 ) IMP:N,P=1  $ Be layer
10    9300 -8.19      -21 20 #(-19 18 ) IMP:N,P=1  $ VV2
12    5014 -1.973     22 -23 #(-21 20 ) &
     #(-48 -52 -23 21 4 #(-24 -51 -23 21 4 ) ) IMP:N,P=1
13    9300 -8.19      25 -26 #(22 -23 ) IMP:N,P=1  $ Tank
18    0               #(25 -26 )-37  IMP:N,P=1  $ Vacuum insulation
19    0               37  IMP:N,P=0  $ Graveyard
20    9300 -4.1       -23 41 -40 -46 IMP:N,P=1 $ Waveguide 1
21    9300 -4.1       46 -47 21 -40 -23 50 IMP:N,P=1 $ Waveguide 2
22    9300 -4.1       44 -43 2 42 -1 IMP:N,P=1 $ Antenna
23    6000 -10.28     50 -49 2 45 -1 #(44 -43 2 42 -1 ) IMP:N,P=1 $ Moly coating
24    6000 -10.28     -48 -52 -23 21 4 #(-23 41 -40 -46 ) & $ Moly coating
     #(46 -47 21 -40 -23 50 )#(-24 -51 -23 21 4 ) IMP:N,P=1

c ********************************************************************
c                    Surface Cards
c
   1      tz 0 0 0 285 208 181
```

```
   2      cz 255
   3      pz -178
   4      pz -50
   5      tz 0 0 0 360 150 83
   6      cz 265.1
   7      tz 0 0 0 367 100 55
   9      tz 0 0 0 375 50 28
c  11       pz 160
  12       cz 254
  13       tz 0 0 0 285 209 182
  14       cz 253
  15       tz 0 0 0 285 210 183
  16       cz 251
  17       tz 0 0 0 285 212 185
  18       cz 250
  19       tz 0 0 0 285 213 186
  20       cz 247
  21       tz 0 0 0 285 216 189
  22       cz 192
  23      rcc 0 0 -276 0 0 552 528 $ Tank
  24       cz 496.9 $ Coating
  25       cz 189  $ Outer bound of Tank
  26      rcc 0 0 -279 0 0 558 531
c  36       rcc 0 0 200 0 0 76 286.1
  37      rcc 0 0 -800 0 0 1600 1000  $ Graveyard
  40       cz 502 $ Waveguide
  41       cz 497 $ Waveguide
  42       tz 0 0 0 285 198 170
  43       pz 7.5 $ Antenna
  44       pz -7.5 $ Antenna
  45       tz 0 0 0 285 197.9 169.9
  46      k/z 0 0 -470 1 0 $ Waveguide
  47      k/z 0 0 -475 1 0 $ Waveguide
  48       cz 502.1 $ Coating
  49       pz 7.6 $ Coating
  50       pz -7.6 $ Coating
  51      k/z 0 0 -469.9 1 0 $ Coating
  52      k/z 0 0 -475.1 1 0 $ Coating

c ============================================================

c Inconel 718 (density = 8.19 g/cm^3)
m9300     028058.88c  0.358908 $ Nickel
          028060.88c  0.138303 $ Nickel
          028061.88c  0.006010 $ Nickel
          028062.88c  0.019159 $ Nickel
```

028064.88c 0.004882 $ Nickel
024050.88c 0.009103 $ Chromium
024052.88c 0.175551 $ Chromium
024053.88c 0.019906 $ Chromium
024054.88c 0.004955 $ Chromium
026054.88c 0.010562 $ Iron
026056.88c 0.167026 $ Iron
026057.88c 0.004006 $ Iron
026058.88c 0.000510 $ Iron
041093.88c 0.032870 $ Niobium
042092.88c 0.002679 $ Molybdenum
042094.88c 0.001670 $ Molybdenum
042095.88c 0.002874 $ Molybdenum
042096.88c 0.003012 $ Molybdenum
042097.88c 0.001724 $ Molybdenum
042098.88c 0.004357 $ Molybdenum
042100.88c 0.001739 $ Molybdenum
022046.88c 0.000988 $ Titanium
022047.88c 0.000901 $ Titanium
022048.88c 0.009113 $ Titanium
022049.88c 0.000679 $ Titanium
022050.88c 0.000667 $ Titanium
013027.88c 0.010738 $ Aluminum
027059.88c 0.001672 $ Cobalt
014028.88c 0.002283 $ Silicon
014029.88c 0.000116 $ Silicon
014030.88c 0.000077 $ Silicon
025055.88c 0.000738 $ Manganese
029063.88c 0.000441 $ Copper
029065.88c 0.000197 $ Copper
006012.88c 0.001449 $ Carbon
015031.88c 0.000187 $ Phosphorus

Appendix B

Data tables for the four tested blankets

In this appendix, we provide the raw TBR, DPA, and helium retention outputs from MNCP for all four blankets and all locations. All helium retention measurements are in atomic parts per million. Poloidal angles are measured in degrees. Total TBR for each location is given in the far left column under the angle in italics.

FLiBe

Region/Poloidal Angle	Quantity	First Wall	Vacuum Vessel 1	Cooling Channel	Beryllium layer	Vacuum Vessel 2	Blanket	Blanket Tank	Waveguides	Antenna
0	*TBR*	-	-	0.2979	0.00174	-	0.7886	-	-	-
1.0882	*DPA*	11.29	33.24	-	-	18.99	-	0.0265	2.20	46.84
	He	2.64	187.94	$4.17x10^4$	2811.3	95.48	$2.26x10^3$	0.1012	3.26	268.40
50	*TBR*	-	-	0.2977	0.00174	-	0.7896	-	-	-
1.0890	*DPA*	11.29	33.23	-	-	18.99	-	0.0272	1.35	43.87
	He	2.64	187.92	$4.17x10^4$	2811.7	95.48	$2.25x10^3$	0.1046	2.24	248.96
75	*TBR*	-	-	0.2976	0.00174	-	0.7905	-	-	-
1.0900	*DPA*	11.30	33.29	-	-	19.03	-	0.0272	0.73	38.73
	He	2.65	188.43	$4.17x10^4$	2819.3	95.75	$2.24x10^3$	0.1043	2.81	213.85
110	*TBR*	-	-	0.2975	0.00176	-	0.7931	-	-	-
1.0924	*DPA*	11.37	33.47	-	-	19.14	-	0.0271	1.58	27.58
	He	2.67	189.97	$4.18x10^4$	2840.5	96.5	$2.25x10^3$	0.1037	5.99	136.28

126	*TBR*	-	-	0.2970	0.00176	-	0.7936	-	-	-
1.0924	*DPA*	11.33	33.40	-	-	19.16	-	0.0271	2.02	25.91
	He	2.66	189.70	$4.18x10^4$	2841.74	96.75	$2.25x10^3$	0.1041	1.94	125.29
147	*TBR*	-	-	0.2972	0.00175	-	0.7917	-	-	-
1.0907	*DPA*	11.30	33.32	-	-	19.08	-	0.0267	3.84	35.08
	He	2.65	188.83	$4.17x10^4$	2928.10	96.19	$2.25x10^3$	0.1022	3.44	191.30
180	*TBR*	-	-	0.2973	0.00174	-	0.7907	-	-	-
1.0898	*DPA*	11.29	33.28	-	-	19.05	-	0.0267	5.67	39.46
	He	2.64	188.47	$4.17x10^4$	2821.6	95.96	$2.25x10^3$	0.1022	4.94	222.36

Table B.1. Raw MCNP output for the FLiBe blanket at all seven launcher poloidal locations.

Pb-17Li

Region/Poloidal Angle	**Quantity**	**First Wall**	**Vacuum Vessel 1**	**Cooling Channel**	**Beryllium layer**	**Vacuum Vessel 2**	**Blanket**	**Blanket Tank**	**Waveguides**	**Antenna**
0	*TBR*	-	-	0.1648	0.00171	-	0.9294	-	-	-
1.0944	*DPA*	13.29	41.36	-	-	26.92	-	0.3617	6.18	54.72
	He	2.65	182.52	$6.46x10^3$	2597.8	88.55	$6.96x10^2$	0.0565	2.45	265.40
50	*TBR*	-	-	0.1648	0.00171	-	0.9293	-	-	-
1.0958	*DPA*	13.29	41.36	-	-	26.94	-	0.3697	4.04	51.55
	He	2.65	182.50	$6.45x10^3$	2599.0	88.53	$6.90x10^2$	0.0576	1.79	246.21
75	*TBR*	-	-	0.1649	0.00172	-	0.9305	-	-	-
1.0971	*DPA*	13.31	41.43	-	-	26.99	-	0.3714	2.22	46.11
	He	2.66	182.97	$6.44x10^3$	2605.1	88.77	$6.85x10^2$	0.0577	2.27	211.37
110	*TBR*	-	-	0.1652	0.00173	-	0.9352	-	-	-
1.1021	*DPA*	13.39	41.66	-	-	27.14	-	0.3685	4.49	34.23
	He	2.68	184.45	$6.48x10^3$	2624.1	89.49	$6.90x10^2$	0.0576	4.04	134.17
126	*TBR*	-	-	0.1650	0.00173	-	0.9355	-	-	-
1.1022	*DPA*	13.32	41.52	-	-	27.08	-	0.3447	7.55	32.98
	He	2.67	184.18	$6.49x10^3$	2624.3	89.71	$6.77x10^2$	0.0557	1.49	123.24
147	*TBR*	-	-	0.1649	0.00172	-	0.9320	-	-	-

1.0986	*DPA*	13.31	41.47	-	-	27.04	-	0.3614	12.22	42.77
	He	2.66	183.33	$6.46x10^{3}$	2612.7	89.18	$6.90x10^{2}$	0.0567	2.54	188.91
180	*TBR*	-	-	0.1648	0.00172	-	0.9296	-	-	-
1.0961	*DPA*	13.30	41.42	-	-	26.99	-	0.3576	16.15	47.40
	He	2.65	182.99	$6.46x10^{3}$	2607.1	88.96	$6.90x10^{2}$	0.0567	3.61	220.09

Table B.2. Raw MCNP output for the Pb-17Li blanket at all seven launcher poloidal locations.

Li_4SiO_4

Region/Poloidal Angle	Quantity	First Wall	Vacuum Vessel 1	Cooling Channel	Beryllium layer	Vacuum Vessel 2	Blanket	Blanket Tank	Waveguides	Antenna
0	*TBR*	-	-	0	0.00218	-	0.9886	-	-	-
0.9908	*DPA*	11.44	33.78	-	-	22.53	-	0.0062	1.92	47.56
	He	2.64	184.83	-	3145.20	113.05	$2.57x10^{3}$	0.0158	2.48	266.60
50	*TBR*	-	-	0	0.00218	-	0.9888	-	-	-
0.9910	*DPA*	11.44	33.77	-	-	22.52	-	0.0062	1.27	44.57
	He	2.64	184.86	-	3145.67	113.06	$2.56x10^{3}$	0.0156	2.07	247.33
75	*TBR*	-	-	0	0.00219	-	0.9891	-	-	-
0.9913	*DPA*	11.45	33.83	-	-	22.57	-	0.0062	0.69	39.44
	He	2.65	185.34	-	3152.4	113.37	$2.55x10^{3}$	0.0157	2.58	212.30
110	*TBR*	-	-	0	0.00221	-	0.9912	-	-	-
0.9934	*DPA*	11.52	34.00	-	-	22.69	-	0.0062	1.58	28.29
	He	2.67	186.83	-	3176.3	114.31	$2.54x10^{3}$	0.0156	5.73	135.04
126	*TBR*	-	-	0	0.00220	-	0.9907	-	-	-
0.9929	*DPA*	11.47	33.93	-	-	22.69	-	0.0061	2.03	26.65
	He	2.66	186.52	-	3173.7	114.48	$2.55x10^{3}$	0.0158	1.61	124.26
147	*TBR*	-	-	0	0.00219	-	0.9895	-	-	-
0.99169	*DPA*	11.45	33.84	-	-	22.61	-	0.0061	3.61	35.84
	He	2.64	185.65	-	3160.0	113.86	$2.54x10^{3}$	0.0160	2.55	190.12
180	*TBR*	-	-	0	0.00219	-	0.9891	-	-	-
0.99129	*DPA*	11.44	33.81	-	-	22.58	-	0.0062	5.13	40.20

	He	2.64	185.31	-	3153.7	113.60	$2.54x10^3$	0.0162	3.37	221.11

Table B.3. Raw MCNP output for the Li_4SiO_4 blanket at all seven launcher poloidal locations.

Li_2TiO_3

Region/Poloidal Angle	Quantity	First Wall	Vacuum Vessel 1	Cooling Channel	Beryllium layer	Vacuum Vessel 2	Blanket	Blanket Tank	Waveguides	Antenna
0	*TBR*	-	-	0	0.00218	-	0.9708	-	-	-
.9730	*DPA*	11.55	34.24	-	-	23.11	-	0.0052	1.95	48.01
	He	2.64	184.84	-	3140.4	112.98	$1.51x10^3$	0.0115	2.31	266.59
50	*TBR*	-	-	0	0.00218	-	0.9707	-	-	-
.9729	*DPA*	11.54	34.23	-	-	23.10	-	0.0051	1.31	45.02
	He	2.64	184.86	-	3140.4	112.98	$1.50x10^3$	0.0114	1.99	247.41
75	*TBR*	-	-	0	0.00219	-	0.9714	-	-	-
.9736	*DPA*	11.56	34.29	-	-	23.14	-	0.0052	0.71	39.83
	He	2.65	185.34	-	3147.9	113.30	$1.49x10^3$	0.0116	2.46	212.30
110	*TBR*	-	-	0	0.00221	-	0.9736	-	-	-
.9758	*DPA*	11.63	34.45	-	-	23.27	-	0.0052	1.63	28.66
	He	2.68	186.82	-	3171.8	114.24	$1.49x10^3$	0.0116	5.49	135.04
126	*TBR*	-	-	0	0.00221	-	0.9730	-	-	-
.9752	*DPA*	11.59	34.39	-	-	23.63	-	0.0051	0.69	27.06
	He	2.66	186.47	-	3169.0	114.34	$1.49x10^3$	0.0116	1.60	124.09
147	*TBR*	-	-	0	0.00220	-	0.9719	-	-	-
.9741	*DPA*	11.56	34.30	-	-	23.19	-	0.0052	3.75	36.22
	He	2.65	185.63	-	3155.3	113.73	$1.49x10^3$	0.0117	6.79	189.68
180	*TBR*	-	-	0	0.00219	-	0.9712	-	-	-
.97339	*DPA*	11.55	34.27	-	-	23.15	-	0.0053	5.25	40.58
	He	2.64	185.27	-	3149.4	113.46	$1.49x10^3$	0.0120	3.08	220.47

Table B.4. Raw MCNP output for the Li_2TiO_3 blanket at all seven launcher poloidal locations.

Appendix C

Example FISPACT input

In this Appendix, we provide an example input file for FISPACT. The input file requires the total energy-integrated flux in n/cm^2/sec, and the material of the region considered. A separate fluxes file with the average cell fluxes from MCNP must also be submitted. The example below is for the tungsten first wall, to be irradiated for seven days.

```
NOHEAD
MONITOR 1
PROJ 1
NOERROR
AINPUT
FISPACT
* IRRADIATION OF ARC FIRST WALL
MASS 4.4648E+4 1
    W   100
DOSE 2 1.1
MIND 1.E5
HAZA
HALF
GRAPH 2 0 1 1 3
FLUX 7.33E+14
ATOMS
LEVEL 100 1
TIME 7 DAYS
TAB2 45
ATWO
ATOMS
LEVEL 20 1
FLUX 0.
ZERO
ATOMS
TIME 10 YEARS ATOMS
END
* END
/
```